A geophysical perspective on Earth's mantle water content: Inverting long-period electromagnetic sounding data using laboratory-based electrical conductivity profiles

A. Khan[1], T. J. Shankland[2]

[1] *Institute of Geochemistry and Petrology, Swiss Federal Institute of Technology, Zürich, Switzerland*

[2] *Geophysics Group, Los Alamos National Laboratory, Los Alamos, USA*

Abstract

This paper applies electromagnetic sounding methods for Earth's mantle to constrain its thermal state, chemical composition, and "water" content. We consider long-period inductive response functions in the form of C-responses from four stations distributed across the Earth (Europe, North America, Asia and Australia) covering a period range from 3.9 to 95.2 days and sensitivity to ∼1200 km depth. Rather than invert C-responses for conductivity profiles, we invert directly for chemical composition and thermal state using a self-consistent thermodynamic method to compute phase equilibria as functions of pressure, temperature, and composition (in the Na_2O-CaO-FeO-MgO-Al_2O_3-SiO_2 model system). Computed mineral modes are combined with recent laboratory-based electrical conductivity models from independent experimental research groups (Yoshino (2010) and Karato (2011)) to compute bulk conductivity structure beneath each of the four stations from which C-responses are estimated. This scheme is interfaced with a sampling-

based algorithm to solve the resulting non-linear inverse problem. The algorithm relies on a Markov chain Monte Carlo method to sample the posterior distribution in the model space from which a range of models fitting the observations within uncertainties are obtained. This approach has two advantages: (1) It anchors temperatures, composition, electrical conductivities, and discontinuities that are in laboratory-based forward models, and (2) At the same time it permits the use of geophysical inverse methods to optimize electrical profiles to match geophysical data. The results show variations in upper mantle temperatures beneath the four stations that appear to persist throughout the upper mantle and parts of the transition zone consistent with observations from seismic tomography images that show major lateral velocity variations in the upper mantle. Calculated mantle temperatures at 410 and 660 km depth lie in the range 1250–1650 °C and 1500–1750 °C, respectively, and generally agree with experimentally-determined temperatures at which the measured phase reactions olivine→β-spinel and γ-spinel→ferropericlase+perovskite occur. The retrieved conductivity structures beneath the various stations also tend to follow trends observed for temperature with the strongest lateral variations in the uppermost mantle, and for depths >300 km appear to depend less on the particular mineral electrical conductivity database. Electrical conductivities ($\log_{10}(\sigma)$) at 410 km depth have lateral variations that range from -3 to -1, while at 660 km depth $\log_{10}(\sigma)$ varies from -2 to -0.5, in overall agreement with purely geophysically-derived global and semi-global one-dimensional conductivity models. Both electrical conductivity databases point to ∼0.001 wt% H_2O in the upper mantle with values ranging from 0.0005–0.002 and 0.0007–0.0013

wt% H_2O for the laboratory databases of Karato (2011) and Yoshino (2010), respectively. However, for transition zone minerals results from the different laboratory databases suggest that a much higher water content is required by the measurements of Yoshino (2010). Further, there is evidence of lateral heterogeneity: The sub-Australian mantle appears "drier" than that beneath southwestern North America, Europe, or Asia.
Keywords: Mantle composition, thermal state, electrical conductivity, water content, electromagnetic sounding, inverse problems

1. Introduction

Electromagnetic sounding (EM) of the Earth has proven a valuable geophysical tool in addition to seismology for probing the physical structure of Earth's mantle. In spite of EM soundings having lower spatial resolution in comparison to seismic methods, they are an important complement to the latter for extracting information on the physical state of Earth's mantle. In principle, electrical methods provide stronger constraints on chemical composition and thermal state because electrical conductivity is more sensitive to variations in mantle chemistry and temperature and hence to mineralogy, than are elastic properties.

In order to examine how parameters such as temperature, chemical components (e.g., Fe, Al, H_2O), defect chemistry, and oxygen fugacity affect conductivity there are complementary laboratory efforts to enlarge the electrical conductivity database (e.g., Yoshino (2010) and Karato (2011) for reviews and compilations of recent measurements). Using electrical conductivity as a means to infer the amount of water stored in the upper mantle and tran-

sition zone (TZ) has been of particular interest (e.g., Huang et al., 2005; Wang et al., 2006; Yoshino et al., 2006, 2008, 2009; Dai & Karato, 2009a,b,c; Manthilake et al., 2009) as even small amounts of water can cause significant changes to the physical properties of mantle minerals (e.g., Karato, 1999; Hirth & Kohlstedt, 1996; Mei & Kohlstedt, 2000; Karato & Jung, 2003; Litasov & Ohtani, 2007; Mao et al., 2008) with potentially strong implications for mantle dynamics (e.g., Bercovici & Karato, 2003; Karato, 2006).

However, to reliably constrain the amount of water in the mantle (henceforth, mantle implies upper mantle and TZ only) requires not only a careful characterization of the influence of various properties on mantle mineral electrical conductivity as measured in the laboratory, but an equal measure of related effort to improve the EM data and conductivity models from which inferences about mantle structure are drawn. This is, however, not an easy task in relation to the abundance of seismic data and their higher resolving power. Constructing the electrical conductivity equivalent of high-resolution global seismic tomography images from long-period EM sounding data has only been undertaken very recently (e.g., Kelbert et al., 2009; Tarits & Mandea, 2010; Kuvshinov & Semenov, 2011; Semenov & Kuvshinov, 2011). These models reveal large lateral variations in electrical conductivity and are in line with evidence from regionalized 1D studies (e.g., Egbert & Booker, 1992; Neal et al., 2000; Jones et al., 2003; Tarits et al., 2004; Khan et al., 2011), semi-global 1D radial profiles (e.g., Olsen, 1999; Utada et al., 2003; Kuvshinov et al., 2005) and 3D semi-global models (e.g., Fukao et al., 2004; Koyama et al., 2006; Utada et al., 2009; Shimizu et al., 2010). However, given the limited spatial resolution of present 3D models, in addition

to problems of data interpretation such as assumed (P_1^0) source geometry, their use for drawing inferences about variations in mantle water content on a global scale is probably premature (see Kuvshinov (2011) for further discussion).

More the to point, knowledge of electrical conductivity by itself only provides hints about underlying properties. A more informative process comes from geophysically-derived electrical conductivity models based on laboratory data following assumptions about composition and temperature (e.g., Xu et al., 2000; Dobson & Brodholt, 2000a; Karato, 2011, Khan et al., 2011). More definitive approaches in which EM data are inverted directly for thermochemical state (e.g., Khan et al., 2006; Verhoeven et al., 2008) are able to cover a much wider parameter range.

The purpose of the present study is to first investigate the extent to which various properties (major element chemistry, water content and temperature) are actually sensed by a set of EM sounding data and then to invert these data for thermochemical state and mantle water content. The first stage is illustrated by comparing simple examples in which electromagnetic inductive responses of various electrical conductivity profiles are constructed by varying in turn water content, composition, and temperature. In the next stage, we invert the EM sounding data for thermochemical state along the lines of a previous investigation (Khan et al., 2006) in which thermodynamic methods (Gibbs free energy minimization) were interfaced with a stochastic sampling algorithm to generate a large collection of one-dimensional conductivity profiles whose EM responses are compared with geophysical observations. We consider two important improvements: 1) a considerably

augmented (in quantity and quality) mineral physics database of laboratory-measured electrical conductivities of upper mantle and TZ minerals obtained by two independent groups (e.g., Yoshino (2010) and Karato (2011)), which will be considered independently so as to minimize bias and 2) high-quality long-period inductive responses recently acquired (Khan et al. 2011) from a set of geomagnetic observatories distributed across the globe (Europe, China, Australia, and North America). The different locales represent distinct tectonic settings spanning regions of continental extension (TUC), relatively young continent (FUR and LZH), and Archean craton (ASP) (Table 1).

2. Long-period electromagnetic sounding data

Data selection and processing have been described in detail in a previous study (Khan et al. 2011). Briefly, the C-responses (defined below) that we consider 1) satisfy quasi-1D behaviour; 2) are located away from polar regions where auroral source effects are of possible influence (Fujii & Schultz, 2002); 3) have high coherency, low uncertainty, and vary smoothly; and 4) cover a large period range (3.9 to 95.2 days). The following stations were found to satisfy the above criteria: Fürstenfeldbrück (FUR), Europe; Langzhou (LZH), China; Alice Springs (ASP), Australia; Tucson (TUC), North America; Honolulu (HON), North Pacific; Hermanus (HER), South Africa. Of these we consider the first four stations for further analysis here, because the latter two are influenced by the ocean induction effect (Kuvshinov et al., 2002), which cannot be modelled thermodynamically. Length of data series and coordinates (geographical and geomagnetic) for the four stations are summarized in Table 1.

Table 1: Summary of geomagnetic observatories.

Station	Latitude	Longitude	Geomag. latitute	Observation period
Fürstenfeldbrück (FUR)	48.17	11.28	48.38	1957 - 2007
Langzhiou (LZH)	36.09	103.85	25.86	1980 - 2007
Alice Springs (ASP)	-23.76	133.88	-32.91	1992 - 2007
Tucson (TUC)	32.17	249.27	39.88	1957 - 1994

Under the assumption of a P_1^0 source structure, C-responses are defined as follows (Banks, 1969)

$$C(\omega) = -\frac{a \tan \vartheta}{2} \frac{Z(\omega)}{H(\omega)} \tag{1}$$

where $a = 6371.2$ km is Earth's mean radius, ϑ geomagnetic co-latitude, $Z(\omega)$ and $H(\omega)$ vertical and horizontal (directed toward geomagnetic north) components of the geomagnetic field, respectively, at frequency $\omega = 2\pi/T$ and period T. This technique is known as the $Z : H$ method (for further details see Khan et al., 2011). As outlined in our previous investigation, the inductive responses provide information on mantle structure to a depth of about 1200 km and, although data are most sensitive in the depth range 500-1000 km, there is considerable sensitivity to upper mantle structure. Finally, the use of 1D radial conductivity profiles for making 3D inferences is also discussed in our previous study.

3. Laboratory electrical conductivity data

Experimental results show that mechanisms of mineral electrical conductivity usually increase with temperature according to an Arrhenius relation

(e.g., Fisler & Tyburczy, 1995)

$$\sigma = \sigma_0 \exp\left(-\frac{H}{kT}\right) \tag{2}$$

where σ_0 is the so-called pre-exponential factor, H activation enthalpy, k Boltzmann's constant, and T is absolute temperature. σ_0 and H both depend on the particular charge transport mechanism. Generally, electrical conductivity of a hydrous iron-bearing silicate mineral is given in terms of several charge transport mechanisms (e.g., Yoshino et al., 2009)

$$\sigma = \sigma_i + \sigma_h + \sigma_p \tag{3}$$

where σ_i, σ_h and σ_p denote contributions from ionic conduction (migration of Mg-site vacancies), small polaron conduction (hopping of electrons between ferric and ferrous iron sites), and conduction arising from migration of protons, respectively.

Several groups have recently measured the electrical conductivity of major upper mantle and TZ minerals with the difficult outcome for the community of obtaining somewhat discrepant results. Whilst the issue has been debated (e.g., Karato & Dai, 2009; Yoshino & Katsura, 2009a; Yoshino, 2010; Karato, 2011), it is yet to be resolved. To minimize any particular bias we have created two electrical conductivity databases that are based on the measurements of 1) Yoshino, Katsura and coworkers (YK) and 2) Karato, Dai and coworkers (KD). These will be briefly summarized below.

Minerals of interest include olivine (ol), orthopyroxene (opx), clinopyroxene (cpx), garnet (gt), the high-pressure polymorph of cpx (C2/c), akimotoite (aki), wadsleyite (wad), ringwoodite (ring), ferropericlase (fp), perovskite (pv), calcium perovskite (ca-pv), and calcium ferrite (cf). It should be noted

that in the case of C2/c, aki, ca-pv, and cf no electrical conductivity measurements are presently available. As in Khan et al. (2006) we use the electrical conductivity of cpx as a proxy for C2/c and aki; for ca-pv we assume conductivity to equal that of Al-free pv, because Al is less soluble in ca-pv than in pv; for cf we disregard the contribution to electrical conductivity in line with an earlier study (Khan et al., 2011), where it was shown that omitting the contribution of a mineral that is present at levels <10 vol%, produces a difference in bulk conductivity of <0.02 log units. In the following we summarize the conductivity data employed here for the above minerals, and unless stated otherwise data parameters have the same meaning as in Eqs. 2 & 3.

3.1. YK database

The electrical conductivity for hydrous iron-bearing olivine can be described by the form (Yoshino et al., 2009)

$$\sigma = \sigma_0^i \exp\left(-\frac{H_i}{kT}\right) + \sigma_0^h \exp\left(-\frac{H_h}{kT}\right) + \sigma_0^p C_w \exp\left(-\frac{H_0 - \alpha C_w^{1/3}}{kT}\right) \quad (4)$$

where the different σ_0s and Hs are pre-exponential factors and activation enthalpies for the various conduction mechanisms, respectively, C_w water content in wt%, and α a geometrical factor. Values for these parameters are in table 3.1

Table 2: Parameters and their sources used to characterize olivine conductivity (after Yoshino et al., 2009).

$\log_{10}(\sigma_i)$	H_i (eV)	$\log_{10}(\sigma_0^h)$	H_h (eV)	$\log_{10}(\sigma_0^p)$	H_0 (eV)	α
4.73±0.53	2.31±0.07	2.98±0.85	1.71±0.04	1.9±0.44	0.92±0.04	0.16±0.02

145

146 For opx and cpx we model electrical conductivity according to Eq. 2 and
147 use the values for σ_0 and H measured by Xu & Shankland (1999). For gt
148 we consider measurements by Yoshino et al. (2008a) and use Eq. 2 as in the
149 case of opx and cpx. Parameter values are given in table 3.

Table 3: Parameters used to characterize conductivities of orthopyroxene (opx), clinopyroxene (cpx) and garnet (gt). For gt no uncertainties were provided in the original data. Parameters are from Xu & Shankland (1999) for opx and cpx, and Yoshino et al. (2008a) for gt.

Mineral	$\log_{10}(\sigma_0)$	H (eV)
opx	3.72±0.1	1.8±0.02
cpx	3.25±0.11	1.87±0.02
gt (<1300K)	1.73	1.27
gt (1300-1750K)	3.03	1.59
gt (>1800K)	4.24	2.02

150 Wadsleyite conductivity is taken from Manthilake et al. (2008) and is
151 given by

$$\sigma = \sigma_0^h \exp\left(-\frac{H_h}{kT}\right) + \sigma_0^p C_w \exp\left(-\frac{H_0 - \alpha C_w^{1/3}}{kT}\right) \quad (5)$$

152 where the first and second terms signify small polaron and proton conduction,
153 respectively. Parameter values are summarized in table 4.

154 For ringwoodite, we consider the measurements by Yoshino et al. (2008b)
155 for proton conduction, while the small polaron term is taken from Yoshino
156 & Katsura (2009b).

$$\sigma = \sigma_0^p C_w \exp\left(-\frac{H_0 - \alpha C_w^{1/3}}{kT}\right) + \sigma_0^{Fe} X_{Fe} \exp\left(-\frac{H_0^{Fe} - \alpha_{Fe} X_{Fe}^{1/3}}{kT}\right) \quad (6)$$

Table 4: Wadsleyite conductivity parameters and their sources (after Manthilake et al., 2008).

σ_0^h (S/m)	H_h (eV)	σ_0^p (S/m)	H_0 (eV)	α
399±311	1.499±0.1	7.749±4.08	0.689±0.03	0.02±0.02

In the Fe correction term, X_{Fe} is mole fraction of Fe in the Mg site, H_0^{Fe} activation enthalpy at very low Fe concentrations, and α_{Fe} a geometrical factor; Yoshino & Katsura (2009b) found two different temperature regimes each with their own parameter values. At high temperatures the Fe correction term becomes negligible compared with the small polaron term. Parameter values are compiled in table 5.

Table 5: Ringwoodite conductivity parameters and their sources. The small polaron term is from Yoshino & Katsura (2009b), whereas the proton conduction term is from Yoshino et al. (2008b).

T (K)	σ_0^p (S/m)	H_0 (eV)	α	σ_0^{Fe} (S/m)	H_0^{Fe} (eV)	α_{Fe}
<1000	27.79±9.6	1.12±0.03	0.67±0.03	467±150	2.14±0.05	2.14±0.07
>1000	27.79±9.6	1.12±0.03	0.67±0.03	10042±4211	2.08±0.06	1.55±0.09

For the major lower mantle minerals ferropericlase and perovskite electrical conductivities are modelled as

$$\sigma = \sigma_0 \exp\left(-\frac{E+PV}{kT}\right) \tag{7}$$

where E, P and V are activation energy, pressure, and activation volume respectively. These parameters were measured by Xu et al. (2000) for ferropericlase and Xu et al. (1998) for both Al-free and Al-bearing perovskite. Data parameters are tabulated in table 6.

Table 6: Parameters used to model ferropericlase (fp) and perovskite (pv) conductivities. Parameters are from Xu et al. (2000) for fp and Xu & Shankland (1998) for pv.

Mineral	$\log_{10}(\sigma_0)$	E (eV)	V (cm^3/mol)
fp	2.69±0.1	0.85±0.03	-0.26
pv (Al-bearing)	1.87±0.11	0.7±0.04	-0.1
pv (Al-free)	1.12±0.12	0.62±0.04	-0.1

In treating upper mantle and transition zone minerals we have omitted pressure effects arising from activation volumes because of the relatively narrow pressure ranges over which the minerals are stable. Although some laboratory experiments have suggested that electrical conductivity of major lower mantle minerals varies with composition (Fe in the case of ferropericlase (Dobson & Brodholt, 2000b; Wu et al., 2010) and Al in the case of perovskite (Xu et al., 1998)), we omit their possible contributions here, given that geophysical data only sense to depths of ∼1200 km.

3.2. KD database

Conductivity data from Karato, Dai and coworkers (Huang et al. (2005), Wang et al., (2006), Dai & Karato (2009a,b,c)) are taken from a recent review (Karato, 2011) and include measurements of ol, opx, gt, wad, and ring. Electrical conductivity of these minerals was described by a relationship of the form

$$\sigma = A_1 \exp\left(-\frac{E_1 + PV_1}{\mathsf{R}T}\right) + A_2 C_w^r \exp\left(-\frac{E_2 + PV_2}{\mathsf{R}T}\right) \qquad (8)$$

where A is a pre-exponential factor, C_w water content in wt%, r an exponent determining water dependence, E activation energy, P pressure, V activation

volume, T temperature, and R the gas constant; subscripts 1 and 2 refer to mechanisms of polaron (1) and proton (2) conduction. Note that effects of oxygen fugacity (f_{O_2}) have been omitted because f_{O_2} is not well-constrained and uncertainties are likely to be small compared to those arising from other parameters (further discussed in next section). The various parameters are tabulated in table 7. For lower mantle minerals we employ equations and parameters summarized in the previous section.

Table 7: Parameters taken from Karato, Dai and coworkers (Karato, 2011) used for modelling conductivity of olivine (ol), orthopyroxene (opx), garnet (gt), wadsleyite (wad) and ringwoodite (ring). Parameter uncertainties are ± 10 kJ/mol for E, ± 0.1 for r and $\pm 0.1/0.3$ (polaron/proton) for $\log_{10} A$

Mineral	$\log_{10} A_1$	$\log_{10} A_2$	r	E_1/E_2 (eV)	V_1/V_2 (cm^3/mol)
ol	2.4	3.1	0.62	154/87	2.4/-
opx	2.7	2.6	0.62	147/82	-/-
gt	2.1	2.7	0.63	128/70	2.5/-0.6
wad	2.1	2.1	0.72	147/88	-/-
ring	-	3.6	0.69	-/104	-/-

3.3. Oxygen fugacity, partial melt, and miscellaneous efects

Most of the above experiments were made at oxygen fugacities controlled by the Mo-MoO_2 buffer (table of 2 of Karato (2011) contains a summary of oxygen fugacities associated with the most recent conductivity experiments). Although it has been observed that olivine conductivity could vary as $f_{O_2}^{1/6}$ (Schock et al., 1989; Duba & Constable, 1993), effects of f_{O_2} under mantle conditions are weakly quantified. As a result we make no corrections for oxy-

gen fugacity to electrical conductivity of the mantle minerals considered here (see also the discussion by Jones et al. (2009)) and thus make the assumption that f_{O_2} throughout the mantle is near that of the Mo-MoO_2 buffer. Moreover, as assessed by Karato (2011), the influence of f_{O_2} on conductivity profiles computed in that study is relatively small given that oxygen fugacity itself varies relatively little. This is also observed when computing olivine conductivity for various oxygen fugacities using SIGMELTS (Pommier & Le Trong, 2011).

As in Xu et al. (2000) and our previous studies no corrections were made for grain boundary effects, given that substantial systematic variations in conductivity are yet to be observed (e.g., Duba & Shankland, 1982; Roberts & Tyburczy, 1993; Xu et al., 2000; ten Grotenhuis et al., 2004; Dai et al., 2008; Watson et al., 2010). The presence of partial melt in the upper mantle (e.g., Shankland & Waff, 1977; Shankland et al., 1981; Roberts & Tyburczy, 1999; Ni et al., 2011) presents another potential concern in view of the scarcity of electrical conductivity measurements pertaining to partial melt (e.g., Tyburczy & Waff, 1983; Gaillard, 2004; Pommier et al., 2010). However, our previous study (Khan et al., 2011) and that of Toffelmier & Tyburczy (2007), who considered the data of Egbert and Booker (1992) for station TUC, showed that partial melt in the upper mantle is not required by EM sounding data. This does not necessarily determine that a thin melt layer is not present within or at the bottom of the uppermost mantle (e.g. Shankland & Waff, 1977; Tauzin et al., 2010), but it means that geophysical data are insensitive to such highly conductive layers should they be present.

Contributions to bulk elecrical conductivity of some minor mineral phases

are not accounted for because of a lack of relevant laboratory measurements. However, disregarding contributions from phases that are present at levels of ∼10 vol% amounts to a negligible difference in bulk conductivity. Specifically, Khan et al. (2011) found that omitting the contribution from the C2/c phase, for example, resulted in a difference of <0.02 log-units, which for practical purposes is insignificant.

Finally, no exhaustive attempt to consider other data sets, e.g., measurements by Romano et al. (2006) on garnet, Romano et al. (2009) on hydrous wadsleyite, Poe et al. (2010) on hydrous olivine, or Wu et al. (2010) on ferropericlase was made and the choice of experimental data possibly influences the outcome. However, because this inversion treatment is able to consider uncertainties in measured electrical conducitivity parameters, it automatically allows for larger variations, and we are thus *a priori* less likely to bias our results.

4. Thermodynamic modelling

In order to compute mantle mineral modes for a given composition X and temperature T, we assume mantle mineralogy to be governed by thermodynamic equilibrium and predict mineralogy as a function of composition, pressure, and temperature by Gibbs energy minimisation using the self-consistent method of Connolly (2005). We adopt the thermodynamic formalism of Stixrude & Lithgow-Bertelloni (2005) as parameterized by Xu et al. (2008) for mantle minerals in the model chemical system Na_2O-CaO-FeO-MgO-Al_2O_3-SiO_2 (abbreviated NCFMAS). The Gibbs energy minimization procedure yields amounts, compositions, and physical properties, including

elastic moduli, of the stable minerals in the model chemical system.

5. Laboratory-based electrical conductivity models

With the data described above we can construct aggregate mantle electrical conductivity profiles. It is necessary to average conductivities of individual minerals with their volume fractions, and there areseveral different schemes to do this in the absence of information on the actual distribution of various mineral phases within the bulk rock.

Of general utility for the calculation of conductivity for multiphase materials are some generalized averages, which include the arithmetic (A) mean (Voigt average), and the harmonic (H) mean (Reuss average)

$$\sigma_{\mathrm{A}} = \sum_{i}^{N} x_i \sigma_i, \quad \sigma_{\mathrm{H}} = \left[\sum_{i}^{N} \frac{x_i}{\sigma_i} \right]^{-1} \tag{9}$$

where σ_i and x_i are conductivity and volume fraction of mineral phase i, respectively, and N is the total number of mineral phases present. The above averages are extremes for upper and lower bounds of bulk conductivity and bracket the permissible range within which the effective conductivity of the multiphase system must be contained (e.g., Waff et al., 1974; Park & Ducea, 2003). It is implictly assumed that x_i is a function of composition, pressure, and temperature, whereas σ_i depends on pressure and temperature as well as Fe and H_2O content.

The Hashin-Shtrikman bounds are considered the narrowest upper and lower bounds for a multiphase system in the absence of knowledge of the geometrical arrangement of the the constituent phases (Hashin & Shtrikman, 1962; Watts et al., 1976; Berryman et al., 1995). The lower bound (HS-)

assumes non-interconnected conductive inclusions within a resistive matrix, and the upper bound (HS+) assumes non-interconnected resistive inclusions in a conductive matrix

$$\sigma_{\mathrm{HS}\pm} = \left[\sum_{i=1}^{N} \frac{x_i}{\sigma_i + 2\sigma_\pm}\right]^{-1} - 2\sigma_\pm \tag{10}$$

where σ_i and x_i are as before conductivity and volume fraction of mineral phase i, respectively, and $\sigma_\pm$ correspond to minimum ($\sigma_- = \min(\sigma_i)$) and maximum ($\sigma_+ = \max(\sigma_i)$) conductivities of the N mineral phases.

In addition to computing bounds we also compute estimators. We consider 1) the geometric mean, 2) the effective medium theory of Landauer (1952) for conducting composites and generalized by Berryman (1995), and 3) the Hill or the Voigt-Reuss-Hill average (Hill, 1963, Watts et al., 1976). The latter average (σ_{VRH}) is the arithmetic mean of the Voigt and Reuss bounds and is biased toward the Voight bound (Shankland & Duba, 1990). The geometric mean (GM) used previously by Shankland & Duba (1990) can readily be computed (e.g., Constable, 2006)

$$\sigma_{\mathrm{GM}} = \prod_i \sigma_i^{x_i}. \tag{11}$$

With more computational effort effective medium theory produces a self-consistent solution (σ_{sc}) that is found through iteration to satisfy (while being bounded by HS- and HS+)

$$\sum_{i=1}^{N} x_i \left[\frac{\sigma_i - \sigma_{\mathrm{sc}}}{\sigma_i + 2\sigma_{\mathrm{sc}}}\right] = 0 \tag{12}$$

The various conductivity bounds and estimates are illustrated in figure 1 for pyrolite composition along the geotherm of Brown & Shankland (1981) using

the YK conductivity database at "dry" mantle conditions. We observe, as in Shankland and Duba (1990), that the only estimator consistently within the Hashin-Shtrikman bounds is σ_{sc}; both σ_{GM} and σ_{VRH} can lie outside these bounds at various points along the bulk conductivity profile. As the Hashin-Shtrikman bounds present the narrowest possible restrictions that exist on an arbitrary isotropic multi-phase system, we consider, like Xu et al. (2000), self-consistently determined conductivity values as the most appropriate average bulk rock conductivity.

Prior to inverting data, we treat some simplified forward models to investigate to what extent the various properties (major element chemistry, temperature, and water content) influence electrical conductivity and, most importantly, C-responses. This approach helps indicate the main consequences of the two databases.

6. Variation in mantle material properties

6.1. Water content

For modelling purposes we consider a homogeneous adiabatic mantle of pyrolite composition (table 9) using the mantle adiabat of Brown & Shankland (henceforth BS adiabat). With this background model, we vary mantle water content for both conductivity databases using the C_ws given in table 8 and compute bulk rock conductivity profiles from the equilibrium mineralogy obtained via Gibbs free energy minization outlined in section 4. The resulting variations in phase proportions and aggregate electrical conductivity for the two databases are shown in figure 2.

For the YK database conductivity variations in the upper mantle are neg-

Table 8: Water contents used for modelling electrical conductivities; water contents are in wt%. Labels a-c are used to identify the conductivity profiles in figure 2. Note that KD provided no conductivity data for ringwoodite at "dry" conditions, and 0 wt% actually implies the presence of a minute amount of water (0.0001 wt%).

Database	C_w^{ol}	C_w^{opx}	C_w^{gt}	C_w^{wad}	C_w^{ring}
YK(a)	0	-	-	0	0
YK(b)	0.001	-	-	0.1	0.1
YK(c)	0.005	-	-	0.5	0.5
KD(a)	0	0	0	0	0
KD(b)	0.001	0.001	0.001	0.1	0.1
KD(c)	0.005	0.005	0.005	0.5	0.5

ligible, whereas differences in the upper and lower TZ are ∼0.3 and ∼0.01 log-units, respectively. Minor conductivity variations in the lower TZ are related to the small contribution arising from the proton conduction term relative to the polaron term (Eq. 6). In contrast, the KD database produces strong conductivity variations in the upper mantle that reach 0.5–1 log-unit, with even stronger variations occuring in the TZ. Comparison of the YK and KD conductivity profiles further accentuates these first-order differences. For the "dry" case, YK is overall more conductive than is KD, with a conductivity decrease across the ol→wad (410-km seismic discontinuity), while KD shows an increase at the same location in addition to a large jump (∼2.5 log-units) at the transition ring→fp+pv (660-km). For the other two "wet" cases the KD conductivity profiles are generally more conductive than the YK profiles over the entire depth range considered here, with relatively strong "410"s and no "660"s, while for the YK profiles the "660" is the strongest

transition (0.5–0.6 log-units). Figure 2 illustrates the important point that in the TZ the KD database requires a smaller water content than does the YK database to achieve the same conductivity increase. With the YK database this appears in the inversion results as requiring a greater water content at the bottom of the upper mantle than does the KD database. For pressures > 25 GPa (corresponding to depths >700 km) the different mantle conductivity profiles converge as expected, because the two databases use the same conductivity data for the lower mantle. Inductive response functions for the six conductivity profiles of figure 2 are shown in figure 3, and we note that while the YK conductivity profiles are almost indistinguishable within the uncertainties of the data, the KD profiles are easily differentiated. For brevity here and in the following two subsections (6.2 and 6.3) only the real part of the inductive response is shown .

Simplifying assumptions made in the present exercise include, in addition to neglecting the contribution from minor mineral phases as discussed previously, disregarding the effect of water on mineral phase equilibria. Although there is evidence that water is likely to stabilize wadsleyite over olivine (e.g., Wood, 1995), scarcity of relevant thermodynamic data prevents us from including this effect. However, given the modest change in electrical conductivity across the ol→wad transition, this is likely a minor issue.

6.2. Major element composition

We consider three different "dry" mantle compositions: 1) harzburgite, 2) pyrolite, and 3) basalt. The compositions are tabulated below (table 9). As before we compute the equilibrium mineralogies for each of these compositions using Gibbs free energy minimization along the BS adiabat. The

resulting electrical conductivities are shown in figure 4.

Table 9: Model endmember bulk compositions in wt%. Basalt and harzburgite compositions are from Khan et al. (2009), whereas the pyrolite composition is taken from Lyubetskaya & Korenaga (2007).

Component	Basalt	Harzburgite	Pyrolite
CaO	13.05	0.5	2.79
FeO	7.68	7.83	7.97
MgO	10.49	46.36	39.5
Al_2O_3	16.08	0.65	3.52
SiO_2	50.39	43.64	44.95
Na_2O	1.87	0.01	0.298

The distinction between computed conductivity profiles is clearly noticeable, which is a direct consequence of the different stable mineralogies produced for each of the three compositions. Again, KD profiles are overall more conductive than their YK counterparts. For the latter, strong conductivity increases only occur at pressures around 18-20 GPa (520-km seismic discontinuity) and ∼23 GPa (660-km). Figure 4 also shows C-responses computed from the six profiles that are distinguishable within the uncertainties of the EM sounding data.

6.3. Geotherm

We consider a homogeneous mantle of pyrolitic composition and combine it with three different geotherms: 1) the BS adiabat (T_{BS}), 2) a "subadiabat" (T_{BS}-150 K), and 3) a "superadiabat" (T_{BS}+150 K). Again we assume a "dry" mantle and compute for each of the geotherms bulk electrical conductivity profiles and inductive response functions (figure 5).

As expected, in the upper mantle there is a quasi-linear variation in conductivity with temperature, given similarity in equilibrium mineralogy among the three different models. This contrasts with the TZ and uppermost lower mantle, where conductivity changes are no longer simply proportional to temperature. Conductivity is seen to vary by ∼0.4 to 1 log-unit in the upper mantle and by ∼0.2-0.3 log-units in the TZ. For a given geotherm KD-based profiles are more conductive than than their YK counterparts. KD-based profiles are distinguished by a strong conductivity increase at the ol→wad transition (∼13 GPa), whereas such a transition is almost absent in YK-based profiles. The opposite occurs at ∼18 GPa (wad→ring transition at ∼520-km) and at ∼23 GPa (ring→fp+pv), where the YK profiles display much stronger increases than do the KD profiles. Electromagnetic response functions for the six profiles are also shown in figure 5 and appear to be distinguishable within uncertainties of response functions.

In summary, these forward-modelling tests have revealed perceptable differences between the two electrical conductivity databases. Most notably, conductivity profiles constructed from the KD-based database are generally more conductive than their YK-based counterparts for a given set of conditions (water content, chemical composition, thermal state). In particular,

KD-based conductivity profiles respond strongly to changes in water content. In comparison, YK conductivity profiles appear generally insensitive to changes in upper mantle and lower TZ water content. Another noticeable difference is the strength of the discontinuous changes in conductivity at major mantle phase transitions. KD-based conductivity profiles generally show strong changes in conductivity at the "410", whereas YK conductivity profiles display relatively strong "520"s and "660"s.

7. Inverse modelling

This section outlines the methodology used to invert the long-period EM sounding data for mantle composition, temperature, and water content. We closely follow the approach of Khan et al. (2006) which supplies details.

In an inverse problem the relationship between model $\mathbf{m}$ and data $\mathbf{d}$ is usually written as

$$\mathbf{d} = \mathrm{g}(\mathbf{m}) \tag{13}$$

where g in the general case is a non-linear operator. However, there is a problem in the absence of an analytical expression for g that would allow us to compute inductive response functions from a knowledge of mantle composition, temperature, and water content. In place of an analytical expression we use an algorithm that, when applied to the various parameters, is able to compute the desired response functions. The workings of the algorithm are given in the scheme below and show the complete decomposition of the forward problem

$$\{X, T, C_w\} \xrightarrow{\mathrm{g}_1} \{M\} \xrightarrow{\mathrm{g}_2} \{\sigma\} \xrightarrow{\mathrm{g}_3} \{\mathrm{Re}(C), \mathrm{Im}(C)\}$$

where X, T and C_w are the fundamental parameters sought, M is equilibrium modal mineralogy, σ is bulk conductivity profile, $\mathrm{Re}(C)$ and $\mathrm{Im}(C)$ real and imaginary parts of inductive response, respectively. The different g's denote the various physical laws, i.e., Gibbs free energy minimization (g_1), construction of bulk laboratory-based conductivity profile (g_2), and prediction of data (g_3).

Central to formulation of a Bayesian approach to inverse problems is extensive use of probability density functions (*pdf*'s) to delineate parameters specific to the problem (Tarantola & Valette, 1982). These include probabilistic prior information on model and data parameters, $f(\mathbf{m})$ (for the present discussion we limit ourselves to a functional dependence on $\mathbf{m}$ and omit any reference to $\mathbf{d}$), and the physical laws that relate data to the unknown model parameters. Using Bayes's theorem these *pdf*'s are combined to yield the postel space

$$\Sigma(\mathbf{m}) = k f(\mathbf{m}) \mathcal{L}(\mathbf{m}), \tag{14}$$

where k is a normalization constant and $\mathcal{L}(\mathbf{m})$ is the likelihood function, which in probabilistic terms can be interpreted as a measure of misfit between observations and predictions from the model $\mathbf{m}$.

We use the Metropolis algorithm (a Markov chain Monte Carlo method) to sample the posterior distribution in the model space using the approach of Mosegaard & Tarantola (1995). While this algorithm is based on a random sampling of the model space, only models that result in a good data fit and that are consistent with prior information are frequently sampled.

Due to the generally complex shape of the posterior distribution, typically employed measures such as means and covariances are generally inadequate

descriptors. Instead we present the solution in terms of a large collection of models sampled from the posterior probability density. In the following section we describe prior information, parameterization, and the likelihood function.

7.1. Prior information

We consider a spherical Earth varying laterally and radially in properties. At the location of each geomagnetic observatory at the Earth's surface, we represent a (local) model of the Earth by a number of layers, corresponding to crust and mantle layers (details given below). The crust is represented by a local physical model, whereas mantle layers are described by model parameters related to composition and temperature. It is implicitly assumed that all parameters depend on geographical position and depth.

7.1.1. Crust

As the long-period EM sounding data considered here are only marginally sensitive to crustal structure we use a simplified parameterization consisting of a crust with the Moho fixed at 50 km depth beneath each station. Crustal conductivity (σ_{cr}) varies independently among the various sites with an interval of 10^{-6} S/m to 10^{-3} S/m and is made to increase with depth down to the Moho.

7.1.2. Mantle Composition

We model the mantle composition using the Na_2-CaO-FeO-MgO-Al_2O_3-SiO_2 (NCFMAS) model system, that accounts for more than 98% of mass of the mantle (Irifune, 1994). Mantle composition is assumed to be uniformly distributed within the bounds given in table 10.

Table 10: Model compositions in wt%.

Component	Mantle
CaO	2.32-3.88
FeO	7.24-8.84
MgO	35-41.6
Al_2O_3	2.92-4.87
SiO_2	40.5-49.4
Na_2O	0.16-0.44

Bounds are chosen such that compositions agree with the range of compositions of mantle peridotites derived from several geochemical studies (table 2 of Lyubetskaya & Korenaga (2007)).

7.1.3. Temperature

We assume mantle temperature to be uniformly distributed with no lower or upper bounds, except for a constant surface temperature of 0°C. We additionally require that temperature not decrease as a function of depth and employ the constraint $T_{j-1} \leq T_j \leq T_{j+1}$ where T_j is temperature in layer j. In this scheme we determine temperature in 25 uniform layers at intervals of 50 km in the depth range 0-700 km and 100 km in the range 700-2886 km; this yields 26 thermal parameters.

7.1.4. Mantle water content

We model water content in the following minerals: olivine, orthopyroxene, garnet, wadsleyite, and ringwoodite and use the simplifying assumption that $C_w^{\mathrm{wad}} = C_w^{\mathrm{ring}}$ because of data sensitivity in the mantle TZ (Khan et al., 2011). Furthermore, we assume that C_ws for all the above minerals are log-uniformly distributed within intervals corresponding to C_w in the range 0 to 1 wt% H_2O. As the KD conductivity measurements do not include measurements for purely "dry" ringwoodite, i.e., a polaron term in Eq. 8 is absent, we set a lower limit of 10^{-4} wt% H_2O for $C_w^{\mathrm{TZ}}(\mathrm{KD})$.

7.1.5. Electrical conductivity parameters

Uncertainties in all parameters relevant to modelling conductivity (e.g., $\sigma_0, H, \alpha, A, r, E$ - see tables 3.1 – 7), are considered by assuming that these are uniformly distributed within bounds of $[p - \Delta p; p + \Delta p]$, where p is any of the aforementioned parameters and Δp the associated uncertainty.

7.1.6. Modal mineralogy and bulk electrical conductivity

Being secondary parameters, i.e., conditional on the values of X, T and C_w, no prior constraints apply to M and σ. This also applies to the conductivity structure of the mid- and lower mantle where data lack sensitivity; core conductivity was fixed to $5{\cdot}10^5$ S/m (Stacey & Anderson, 2001).

7.1.7. Overall parameterization

In summary, we use 35 parameters to describe the crustal and mantle structure beneath each of the four stations modelled here. Given values of these parameters, we compute equilibrium modal mineralogy and bulk electrical conductivity at 75 depth nodes from the surface downward as a function

of pressure, temperature, and composition at intervals of 10 km in the range 50–110 and 570–630 km depth, 20 km in the ranges 110–370, 420–540 and 700–800 km depth, 5 km within the range 380–420, 545–570 and 645–700 km depth, 100 km in the range 800–1600 km depth, and finally 200 km in the depth range from 1600 to 2000 km.

There is no unique way to parameterize the model system, and the particular parameterization chosen here has been found by conducting many trial inversions and reflects a particular, near-minimal, parameterization that yields data being fit within uncertainties. Also, as we have neglected uncertainties of measured mineral physics parameters related to the thermodynamic formulation, actual uncertainties are likely larger than indicated here.

7.2. Posterior distribution

Assuming that data noise can be modeled using a gaussian distribution and that observational uncertainties and calculation errors between the real and imaginary part of the C-response functions are independent, the likelihood function is given by

$$\mathcal{L}(\mathbf{m}) \propto \exp(-\sum_i \frac{[{}_i d_{obs}^{\mathrm{Re}\{C\}} -_i d_{cal}^{\mathrm{Re}\{C\}}(\mathbf{m})]^2}{2_i \Delta_{\mathrm{Re}\{C\}}^2} + \frac{[{}_i d_{obs}^{\mathrm{Im}\{C\}} -_i d_{cal}^{\mathrm{Im}\{C\}}(\mathbf{m})]^2}{2_i \Delta_{\mathrm{Im}\{C\}}^2}) \quad (15)$$

where $d_{obs}^{\mathrm{Re}\{C\}}$, $d_{obs}^{\mathrm{Im}\{C\}}$, $d_{cal}^{\mathrm{Re}\{C\}}$ and $d_{cal}^{\mathrm{Im}\{C\}}$ denote observed and calculated real and imaginary C-responses, respectively, and $\Delta_{\mathrm{Re}\{C\}}$ and $\Delta_{\mathrm{Im}\{C\}}$ are the uncertainties on either of these.

Sampling proceeded by randomly perturbing either of the parameters in the set $\{X,\ T,\ C_w,\ \sigma_{cr}\}$ according to the prior distribution as defined in section 6.1 (for brevity we leave aside parameters pertaining to measurement uncertainties $(\sigma_0, A, H, \alpha, E, V)$. The burn-in time for this distribution

(number of iterations until samples were retained from the posterior distribution) was found to be of the order of $5{\cdot}10^4$. We sampled 1 million models, with an overall acceptance rate of about 35% of which every 100th model was retained for further analysis.

8. Results and Discussion

8.1. Thermal structure

Figure 6 shows the retrieved thermal structure beneath the four stations and reveals mantle temperatures that span a range of 200–250°C to a depth of about 800–900 km. Generally, we observe that sampled geotherms remain relatively well-defined in comparison to prior models over most of the depth range shown here except for lower mantle temperatures beneath station LZH, which are seen not to be well-constrained for depths below 900 km. Comparison of the various thermal profiles obtained from inversion of the two databases are found to be remarkably consistent showing, within uncertainties of the models, the same features including mantle temperatures. This is an important result as it shows that inverting EM sounding data directly for mantle thermal state is to first order independent of the conductivity database employed to model bulk conductivity profiles.

For comparison with the inverted geotherms we include data on upper mantle temperatures from petrological experiments on mineral phase transitions in the system $(Mg,Fe)_2SiO_4$. Ito and Takahashi (1989) found that the ol→wad and ring→fp+pv reactions (410- and 660-km) occured at temperatures of ∼1750±100 K and ∼1900±150 K, respectively. In similar experiments Katsura et al. (2004) determined temperatures of 1760±45 K and

1860±50 K for these reactions, respectively. The inversions are in overall agreement with these experiments. Moreover, temperatures beneathe the various localities follow surface tectonics to some extent in that the Archean craton (ASP) is generally found to be cold relative to a younger continental site (LZH).

8.2. Electrical conductivity structure

Conductivity structures obtained from inversion of long-period inductive response functions discussed in section 2 are shown in figure 7 and their fits to observed data are shown in figures 8 and 9. Calculated inductive response functions from both databases are seen to fit the observations equally well, with no real apparent differences. The non-monotonic increase seen in the real part of the observed C-responses at stations ASP and LZH are incompatible with the assumption of a 1-D conductivity structure (Weidelt, 1972), which likely reflects violation of assumed source structure (P_1^0) and/or possible contamination from the core in the period range in question. Note also that for stations LZH and ASP uncertainties increase at longer periods because of a shorter time span over which data were collected. These points were discussed further in Khan et al. (2011). We omit prior sampled conductivity models in figure 7, as conductivity is a secondary parameter and conditional on the primary parameters (mantle composition and temperature). As previously, we find that relative to the range of prior models, the posterior range is much reduced. Data are not sensitive to crustal structure so that models are shown from the lithosphere on down.

The inversion-derived conductivity profiles beneath the four stations differ markedly as observed earlier (Khan et al., 2011), and although sampled

upper mantle conductivity models span a large range, an order of magnitude variation in conductivity is apparent to ∼400 km depth. As in the previous study, we note that TUC and LZH are more conductive in the upper mantle than are ASP and FUR, which conforms with the real part of the inductive response functions for periods ($\leq 10^6$ s), i.e., $\mathrm{Re}(C_{ASP,FUR}) > \mathrm{Re}(C_{LZH,TUC})$. This observation is also consistent with expected temperature differences. Large variations in electrical conductivity have also been observed in other regionalized 1-D conductivity studies (e.g., Schultz and Larsen, 1987; Egbert and Booker, 1992; Lizzaralde et al., 1995; Neal et al., 2000; Tarits et al., 2004). Within the TZ and lower mantle, in particular, model discrepancies tend to narrow as they do in global seismic tomography models that display large lateral velocity heterogeneities to ∼250 km depth below which they generally become more homogeneous (e.g., Panning & Romanowicz, 2006; Kustowski et al., 2008; Ritsema et al., 2011).

Further comparison of the models constructed from the two laboratory conductivity databases (figure 7) reveals a number of important differences. KD-based profiles are overall observed to be more conductive than their YK counterparts by almost an order of magnitude down to ∼300 km depth. Profiles beneath stations TUC and LZH using the KD database are consistently >0.01 S/m, whereas the equivalent YK-based profiles are <0.01 S/m. Moreover, the highly conductive uppermost upper mantle, which is a distinct feature of the KD-TUC and KD-LZH profiles, also appears somewhat at odds with the purely conductivity-derived models shown in figure 7. This anomalously high conductivity is related to the strong increase in conductivity of hydrous ol and especially of hydrous opx for even small amounts

of water that is an inherent feature of the KD database (figure 2). Another curious feature of KD-based profiles for TUC and LZH is the strong conductivity decrease that occurs just beneath ∼300 km. Neither of the other two KD-based profiles (ASP and FUR) show such a marked behaviour, hence the drops could be related to the above-mentioned high conductivities for depths (<300 km) beneath TUC and LZH. Although low-conductivity bands are somewhat peculiar, they cannot be construed as *a priori* evidence against applying the KD database; they nonetheless suggest that the latter might be used with caution.

In agreement with previous models, all upper mantle conductivities are generally lower than 0.1 S/m. Within the TZ conductivity is observed to increase slightly so as to attain ∼0.1 S/m at the base of the TZ beneath all four stations. A consistent feature of all YK-based profiles is the jump in conductivity at ∼520–540 km depth, which is related to the mineral transformation wad⟶ring. This feature is not produced in KD-based profiles. In the case of KD-FUR, conductivity appears to actually have a slight decrease here. Because eq. 8 lacks any conduction mechanism other than the single proton term, its ability to represent TZ conductivity is restricted.

Across the 660-km discontinuity (ring⟶fp+pv) conductivity increases abruptly by about one order of magnitude to 1 S/m for both databases. Further strong conductivity jumps are not observed in the lower mantle (to 1300 km depth), and conductivity increases only to a minor extent to ∼2-7 S/m. As expected for the lower mantle, differences between conductivity profiles beneath all four stations are minimal because both databases employ the same measurements for pv and fp.

For comparison we also show the conductivity-derived sub-continental European conductivity model of Olsen (1999) and global model of Kuvshinov & Olsen (2006), the laboratory-based models of Xu et al. (2000) and Khan et al. (2006), as well as models from a recent study (Khan et al., 2011). Unlike purely geophysically-derived models, which are characterized by continuous conductivity increase through the mantle, these new profiles resemble earlier laboratory-based models with pronounced discontinuities across major phase transitions. The general inability of EM fields to sense discontinuities is a direct result of their diffusive nature as can be seen by comparing conductivity models obtained here with those of, e.g., Khan et al. (2011). Major differences between present and previous profiles are principally in the upper mantle and are mainly related to differing modelling aspects such as inversion for conductivity only, $d\sigma(r)/dr \geq 0$, and data sensitivity, among others. We should mention that the models of Xu et al. (2000) and Khan et al. (2006) also display a strong jump in electrical conductivity in the vicinity of the seismic 410-km discontinuity (ol$\longrightarrow$wad). This particular increase is not observed here because of using different mineral conductivity databases for major minerals, especially ol and wad. On the basis of measurements performed entirely on nominally anhydrous minerals, Xu et al. (2000) measured a conductivity increase by at least an order of magnitude on going from ol to wad. In contrast, for a given constant upper mantle and TZ water content, the most recent experiments (YK) on hydrous equivalents hint at a smooth conductivity curve on crossing the 410-km discontinuity, while the anhydrous case suggests a decrease in conductivity (figure 2).

8.3. Mantle water content

Compositional variations can also play an important role in determining the electrical conductivity structure (figures 2 - 4). We limit ourselves to discussing variations in upper mantle and TZ water content because data sensitivity to variations in major element composition is relatively minor given the somewhat narrow prior bounds on major element chemistry (table 7). Apart from the indirect dependence of conductivity on composition through the influence of modal mineralogy, we presently only model a direct compositional dependence of conductivity through Eq. 6, which relates ringwoodite conductivity to Fe content as observed in the experiments of Yoshino and Katsura (2009).

Calculated mantle water content is shown in figure 10. In the upper mantle C_w lies in the range 0.0005–0.0015 wt% beneath all four stations. Although minor variations occur for C_w^{ol}, both databases point to a C_w^{ol} ∼0.001 wt%, with a somewhat larger variation in the case of the KD database. For opx and gt (KD database only) C_ws in the range 0.0005–0.0015 wt% are also observed, with a slight tendency for a higher C_w^{gt} relative to C_w^{opx}. These results largely agree with geochemical analyses of mantle rocks, which have found water contents in the range from 0.0002 to 0.05 wt% (e.g., Hirschmann, 2006). The petrologically determined water content, however, might not be representative of that in deeper rocks as samples derive from depths shallower than ∼200 km. In the TZ discrepancies between the two laboratory databases become apparent with C_w^{TZ} <0.005 wt% for the KD database, whereas C_w^{TZ} lies in the range 0.01–0.2 wt% for the YK database (assuming $C_w^{\mathrm{wad}} = C_w^{\mathrm{ring}}$).

Using the YK database, Manthilake et al. (2009) concluded that a "dry" mantle model, i.e., a conductivity profile with C_w=0 wt% throughout, agreed well with current semi-global conductivity profiles and thus, that the concept of a globally hydrated mantle TZ need not be invoked to explain mantle conductivity. On the other hand, Karato (2011), concluded on the basis of the KD database that the average water contents in the uppermost mantle and TZ are around 0.01 and 0.1 wt%, respectively. We tested these inferences by inverting the EM data set from station TUC, while fixing C_w at 0 wt% throughout the mantle. The results (omitted for brevity) revealed that when using the YK database, inverted geotherms and conductivity profiles are essentially unchanged from the "wet" models. Because the YK database is not very sensitive to variations in TZ water content (see section 5.1.1 and the relatively flat posterior distributions of C_w^{TZ} in figure 10F—excepting ASP), a "dry" TZ does not produce a distinctly different inductive response (figure 3). This, however, is not the case for the KD database. Here, a strong trade-off occurs with sampled geotherms, such that unrealistically high mantle temperatures are needed to fit data for a "dry" mantle (e.g., 1800–1900 °C at 410 km depth and 1850–1950 °C at 660 km depth in comparison to 1300–1500 °C (410 km) and 1500–1700 °C (660 km) for the "wet" case). The "dry" case temperatures are several hundred degrees above the experimental temperatures for these phase transitions.

Thus, one observation of these treatments is that within the uncertainties of the two laboratory datasets an uppermost mantle with ∼0.001 wt% H_2O is consistent with both conductivity databases. Another observation is that according to the KD database the TZ should have a comparable water con-

tent of ∼0.001 wt% H_2O in contrast with results from the YK database of values that range from ∼0.03 wt% (ASP) to ∼0.2 wt%. Although tentative, a third observation is an indication of lateral variation: ASP appears to be consistently drier in all but the olivine-dominated regimes.

Reasons for discrepancies between present and earlier forward calculations (e.g., Manthilake et al., 2009; Karato, 2011) are most likely related to 1) the simplified nature of previous laboratory-based conductivity profiles (e.g., adiabatic geotherm, PREM-like pressure profile, mineralogy based on pyrolite composition) and 2) the largely qualitative comparison of these laboratory-based profiles with previous geophysically-derived conductivity profiles.

9. Summary and Conclusion

This study uses a geophysical approach to estimating mantle composition (major element chemistry and water content) and thermal state by inverting a set of long-period electromagnetic sounding data beneath four geomagnetic stations distributed across the globe at diverse tectonic settings. The connection between geophysical observables, physical rock properties (electrical conductivity), and thermo-chemistry is contained in the use of a self-consistent thermodynamic modelling scheme of mantle mineral phase equilibria that depend only on composition, temperature, and pressure. Using inverse methods in the form of a stochastic-based algorithm, we sample these parameters to produce conductivity profiles fitting data within uncertainites to obtain models of mantle conditions that simultaneously combine features of both laboratory and geophysical data.

The results indicate that the thermo-chemical state of the mantle can

be reasonably well-retrieved given a set of high-quality inductive response functions and a consistent set of laboratory mineral conductivity measurements. Concerning the latter, we considered independently the conductivity measurements from two experimental laboratories in order to minimize bias. The independent inversions using either database revealed similar features in mantle temperature structure beneath the four stations and are observed to be in excellent agreement with experimentally-determined temperatures of major mantle phase transitions. The bulk electrical conductivity profiles constructed from the thermo-chemical models were also found to broadly concur with geophysically-derived and previous laboratory-based electrical conductivity profiles. With regard to water content the results imply around 0.001 wt% H_2O in the upper mantle, independent of the particular conductivity database employed. On the other hand, in the TZ much "wetter" (0.001–0.2 wt%) minerals can fit the C-response data.

While this study has shown that it is indeed feasible to constrain mantle thermo-chemical state from inversion of long-period electromagnetic response functions, advancing the understanding of the role played by water in shaping mantle processes nonetheless rests on some key factors that will need to be considered in the future. Of main importance are 1) continued collection and refinement of the laboratory-based mineral electrical conductivity database, 2) construction of high-quality inductive response functions of high coherency and small uncertainties, and not least 3) a continued effort to extend the thermodynamic database employed in modelling mantle mineral phase equilibria. For point 2) it includes extending the observed period range to improve sampling of both the uppermost mantle and the lower man-

tle, while improving sensitivity throughout by decreasing data uncertainties, which presently limit the amount of inferences that can be drawn. Similarly, an improved experimental database for lower mantle conductivity is needed.

In spite of any shortcomings of the analysis here due to absence or scarcity of appropriate experimental data, it is the contention here that a quantitative approach in which geophysical data are tested directly for fundamental parameters (composition and temperature) should be emphasized over approaches that rely on a simplified comparison between geophyical models and forward models constructed from laboratory measurements.

References

[1] Banks, R., 1969. Geomagnetic variations and the electrical conductivity of the upper mantle. Geophys. J. R. Astr. Soc. 17, 457.

[2] Bercovici, D., Karato, S.-I., 2003. Whole-mantle convection and the transition-zone water filter. Nature 425, 39.

[3] Berryman, J.G., 1995. Mixture theories for rock properties. In: American Geophysical Union Handbook of Physical Constants. Ahrens, T.J. (Ed.), AGU, New York, 205.

[4] Brown, J.M., Shankland, T.J. 1981. Thermodynamic parameters in the Earth as determined from seismic profiles. Geophys. J. Roy. Astron. Soc. 66, 579.

[5] Connolly, J. A. D., 2005. Computation of phase equilibria by linear programming: A tool for geodynamic modeling and an application to subduction zone decarbonation. Earth Planet. Sci. Lett. 236, 524.

[6] Constable, S., 2006. SEO3: A new model of olivine electrical conductivity. Geophys. J. Int. 166, 435.

[7] Dai, L., Li, H., Hu., H., Shan, S., 2008. Experimental study of grain boundary electrical conductivities of dry synthetic peridotites under high temperature, high-pressure, and different oxygen fugacity conditions. J. Geophys. Res. 113, B12211, doi:10.1029/2008JB005820.

[8] Dai, L., Karato, S.-I., 2009a. Electrical conductivity of orthopyroxene: implications for the water content of the asthenosphere. Proc. Jpn. Acad. 85, 466.

[9] Dai, L., Karato, S.-I., 2009b. Electrical conductivity of pyrope-rich garnet at high temperature and pressure. Phys. Earth Planet. Int. 176, doi:10.1016/j.pepi.2009.04.002.

[10] Dai, L., Karato, S.-I., 2009c. Electrical conductivity of wadsleyite at high temperatures and high pressure. Earth Planet. Sci. Lett. doi:10.1016/j.epsl2009.08.012.

[11] Dobson, D.P., Brodholt, J.P., 2000a. The electrical conductivity and thermal profile of the Earth's mid-mantle. Geophys. Res. Lett. 27, 2325.

[12] Dobson, D.P, Brodholt, J.P., 2000b. The electrical conductivity of the lower mantle phase magnesiowüstite at high temperatures and pressures. J. Geophys. Res. 105, 531.

[13] Duba, A.G., Shankland, T.J., 1982. Free carbon and electrical conductivity in the Earth's mantle. Geophys. Res. Lett. 9, 1271, doi:10.1029/GL009i011p01271.

[14] Duba, A.G., Constable, S., 1993. The electrical conductivity of lherzolite. J. Geophys. Res. 98, 11885.

[15] Egbert, G., Booker, J.R., 1992. Very long period magnetotellurics at Tucson observatory: Implications for mantle conductivity. J. Geophys. Res. 97, 15099.

[16] Fujii I., Schultz, A., 2002. The 3D electromagnetic response of the Earth to ring current and auroral oval excitation. Geophys. J. Int. 151, 689.

[17] Fukao, Y., Koyama, T., Obayashi, M., Utada, H., 2004. Trans-Pacific temperature field in the mantle transition region derived from seismic and electromagnetic tomography. Earth Planet. Sci. Lett. 217, 425.

[18] Gaillard, F., 2004. Laboratory measurements of electrical conductivity of hydrous and dry silicic melts under pressure. Earth Planet. Sci. Lett. 218, 215, doi:10.1016/S0012-821X(03)00639-3.

[19] Hashin, Z., Shtrikman, S., 1962. A variational approach to the theory of effective magnetic permeability of multiphase materials. J. Appl. Phys. 33, 3125.

[20] Hill, R., 1963. The elastic behaviour of crystalline aggregate. J. Mech. Phys. Solids. 11, 357.

[21] Hirschmann, M.M., Tenner, T., Aubaud, C., Withers, A.C., 2008. Dehydration melting of nominally anhydrous mantle: the primacy of partitioning. Phys. Earth Planet. Int. 176, 54.

[22] Hirth, G., Kohlstedt, D. L., 1996. Water in the oceanic upper mantle: implications for rheology, melt extraction and the evolution of the lithosphere. Earth Planet. Sci. Lett. 144, 93.

[23] Huang, X., Xu, Y., Karato, S.-I., 2005. Water content in the transition zone from electrical conductivity of wadsleyite and ringwoodite. Nature 434, 746.

[24] Ito, E., Takahashi, E., 1989. Postspinel transformations in the system Mg_2SiO_4-Fe_2SiO_4 and some geophysical implications. J. Geophys. Res. 94, 10637.

[25] Jones, A.G., Lezaeta, P., Ferguson, I.J., Chave, A.D., Evans, R., Garcia, X., Spratt, J., 2003. The electrical structure of the Slave craton. Lithos 71, 505.

[26] Jones, A.G., Evans, R.L., Eaton, D.W., 2009. Velocity-conductivity relationships for mantle mineral assemblages in Archean cratonic lithosphere based on a review of laboratory data and Hashin-Shtrikman extremal bounds. Lithos 109, 131, doi: 10.1016/j.lithos.2008.10.014.

[27] Karato, S.-I., 1990. The role of hydrogen in the electrical conductivity of the upper mantle. Nature 347, 272.

[28] Karato, S.-I., 2006. Influence of hydrogen-related defects on the electrical conductivity and plastic deformation of mantle materials: a critical review. In: Jacobsen, S.D., van der Lee, S., (Eds.), Earth's deep water cycle. AGU, Washington DC., 113.

825 [29] Karato, S.-I., 2011. Water distribution across the mantle transition zone
826 and its implications for global material circulation. Earth Planet. Sci. Lett.,
827 301, doi:10.1016/j.epsl.2010.1.038.

828 [30] Karato, S.-I., Jung, H., 2003. Effects of pressure on high-temperature
829 dislocation creep in olivine polycrystals. Philos. Mag. A. 83, 401.

830 [31] Karato, S.-I. & L. Dai, 2009. Comments on "Electrical conductivity of
831 wadsleyite as a function of temperature and water content" by Manthilake
832 et al. Phys. Earth Planet. Int., doi:10.1016/j.pepi.2009.01.011.

833 [32] Katsura, T., et al. 2004. Olivine-wadsleyite transition in the system
834 (Mg,Fe)2SiO4. J. Geophys. Res. 109, B02209, doi:10.1029/2003JB002438.

835 [33] Kelbert, A., Schultz, A., Egbert, G., 2009. Global electromagnetic in-
836 duction constraints on transition-zone water content variations. Nature
837 460, doi:10.1038/nature08257.

838 [34] Khan, A., Connolly, J. A. D., Olsen, N., 2006. Constraining the compo-
839 sition and thermal state of the mantle beneath Europe from inversion of
840 long-period electromagnetic sounding data. J. Geophys. Res. 111, B10102,
841 doi:10.1029/2006JB004270.

842 [35] Khan, A., Boschi, L., Connolly, J.A.D., 2009. On mantle chem-
843 ical and thermal heterogeneities and anisotropy as mapped by in-
844 version of global surface wave data. J. Geophys. Res. 114, B09305,
845 doi:10.1029/2009JB006399.

846 [36] Khan, A., Kuvshinov, A., Semenov, A., 2011. On the heterogeneous

electrical conductivity structure of the Earth's mantle with implications for transition zone water content. J. Geophys. Res. 116, B01103, doi:10.1029/2010JB007458.

[37] Kohlstedt, D.L., Keppler, H., Rubie, D.C., 1996. Solubility of water in the α, β and γ phases of $(Mg,Fe)_2SiO$. Contrib. Miner. Petrol. 123, 345.

[38] Koyama T., Shimizu, H., Utada, H., Ichiki, M., Ohtani, E., Hae, R., 2006. Water content in the mantle transition zone beneath the North Pacific derived from the electrical conductivity anomaly. In: Earth's Deep Water Cycle. Geophys. Monogr. Ser., vol. 168, eds. Jacobsen, S. and S. van der Lee, AGU, Washington DC., 171,

[39] Kustowski, B. Ekström, G., Dziewonski, A.M., 2008. Anisotropic shear-wave velocity structure of the Earth's mantle: A global model. J. Geophys. Res. 113, B06306, doi: 10.1029/2007JB005169.

[40] Kuvshinov, A., 2011. Deep Electromagnetic Studies from Land, Sea, and Space: Progress Status in the Past 10 Years. Surveys in Geophysics. doi: 10.1007/s10712-011-9118-2.

[41] Kuvshinov A., Olsen, N., 2006. A global model of mantle conductivity derived from 5 years of CHAMP, Ørsted, and SAC-C magnetic data. Geophys. Res. Lett. 33, L18301, doi:10.1029/2006GL027083.

[42] Kuvshinov, A., Semenov, A., 2011. Global 3-D imaging of mantle conductivity based on inversion of ground-based C-responses: I. An approach and its verification. Manuscript in preparation.

[43] Kuvshinov, A. V., Olsen, N., Avdeev, D.B., Pankratov, O.V., 2002. Electromagnetic induction in the oceans and the anomalous behaviour of coastal C-responses for periods up to 20 days. Geophys. Res. Lett. 29, doi:10.1029/2001GL014,409.

[44] Kuvshinov, A., Utada, H., Avdeev, D.B., Koyama, T., 2005. 3-D modeling and analysis of D_{st} C-responses in the north pacific ocean region, revisited. Geophys. J. Int. 160, 505.

[45] Landauer, R., 1952. The electrical resistance of binary metallic mixtures. J. Appl. Phys. 23, 779.

[46] Litasov, K.D., Ohtani, E., 2007. Effect of water on the phase relations in Earth's mantle and deep water cycle. In: Ohtani, E., (Ed.), Advances in high-pressure mineralogy. Geological Soc. Amer., p. 115.

[47] Lizzaralde, D., Chave, A., Hirth, G., Schultz, A., 1995. Northeastern Pacific mantle conductivity profile from long-period magnetotelluric sounding using Hawaii to California submarine cable data. J. Geophys. Res. 100, 17837.

[48] Lyubetskaya, T., Korenaga, J., 2007. Chemical composition of Earth's primitive mantle and its variance: 1. Method and results. J. Geophys. Res. 112, B03211, doi:10.1029/2005JB004223.

[49] Manthilake, M., Matsuzaki, T., Yoshino, T., Yamashita, S., Ito, E., & Katsura, T., 2009. Electrical conductivity of wadsleyite as a function of temperature and water content. Phys. Earth Planet. Int., doi:10.1016/j.pepi.2008.06.001.

892 [50] Mao, Z., et al., 2008. Elasticity of hydrous wadsleyite to 12 GPa: Im-
893 plications for Earth's transition zone. Geophys. Res. Lett. 35, L21305,
894 doi:10.1029/2008GL035618.

895 [51] Mei, S., Kohlstedt., D.L., 2000. Influence of water on plastic deformation
896 of olivine aggregates, 2. Dislocation creep regime. J. Geophys. Res. 105,
897 21471.

898 [52] Mosegaard, K., Tarantola, A., 1995. Monte Carlo sampling of solutions
899 to inverse problems. J. Geophys. Res. 100, 12431.

900 [53] Neal, S.L., Mackie, R.L., Larsen, J.C., Schultz, A., 2000. Variations in
901 the eletrical conductivity of the upper mantle beneath North America and
902 the Pacific Ocean. J. Geophys. Res. 105, 8229.

903 [54] Ni, H., Keppler, H., Behrens, H., 2011. Electrical conductivity of hy-
904 drous basaltic melts: implications for partial melting in the upper mantle.
905 Contrib. Mineral. Petrol. doi:10.1007/s00410-011-0617-4.

906 [55] Olsen, N., 1999. Long-period (30 days-1 year) electromagnetic sound-
907 ing and the electrical conductivity of the lower mantle beneath Europe.
908 Geophys. J. Int., 138, 179.

909 [56] Panning, M., Romanowicz, B., 2006. A three-dimensional radially
910 anisotropic model of shear velocity in the whole mantle. Geophys. J. Int.
911 167, 361.

912 [57] Park, S.K., Ducea, M.N., 2003. Can in situ measurements of mantle
913 electrical conductivity be used to infer properties of partial melts ? J.
914 Geophys. Res. 108, 2270, doi:10.1029/2002JB001899.

[58] Poe, B., Romano, C., Nestola., F., Smyth, J.R., 2010. Electrical conductivity anisotropy of dry and hydrous olivine at 8 GPa. Phys. Earth Planet. Int. 181, 103.

[59] Pommier, A., Gaillard, F., Malki, M., Pichavant, M., 2010b. Reevaluation of the electrical conductivity of silicate melts. Amer. Min. 95, 284.

[60] Pommier, A., Le Trong, E., 2011. "SIGMELTS": A web portal for electrical conductivity calculations in geosciences. Computers & Geosciences, in press.

[61] Ritsema, J., van Heijst, H.J., Deuss, A., Woodhouse, J.H., 2011. S40RTS: a degree-40 shear velocity model for the mantle from new Rayleigh wave dispersion, teleseismic traveltimes, and normal-mode splitting function measurements. Geophys. J. Int. 184, doi:10.1111/j.1365-246X.2010.04884.x.

[62] Romano, C., Poe, B., Kreidie, N., C. McCammon, C., 2006. Electrical conductivities of pyrope-almandine garnets up to 19 GPa and 1700°C. Am. Miner. 91, 1371.

[63] Romano, C., Poe, B. T., Tyburczy, J., Nestola, F., 2009. Electrical conductivity of hydrous wadsleyite. European Journal of Mineralogy, 21(3), 615-622.

[64] Roberts, J.J., Tyburczy, J.A., 1993. Impedance spectroscopy of single and polycrystalline olivine: Evidence for grain boundary transport. Phys. Chem. Miner. 20, 19, doi:10.1007/BF00202246.

[65] Roberts, J.J., Tyburczy, J.A., 1999. Partial-melt electrical conductivity: Influences of melt composition. J. Geophys. Res. 104, 7055.

[66] Shimizu H., Utada, H., Baba, K., Koyama, T., Obayashi, M., Fukao, Y., 2010. Three-dimensional imaging of electrical conductivity in the mantle transition zone beneath the North Pacific Ocean by a semi-global induction study. Phys. Earth Planet. Int. 183, doi:10.1016/j.pepi.2010.01.010.

[67] Schultz, A., Larsen, J.C., 1987. On the electrical conductivity of the mid-mantle: I. Calculation of equivalent scalar magnetotelluric response functions. Geophys. J. R. Astron. Soc. 88, 733.

[68] Semenov, A., Kuvshinov, A., 2011. Global 3-D imaging of mantle conductivity based on inversion of ground-based C-responses: II. Results. Manuscript in preparation.

[69] Shankland, T.J., Waff, H.S., 1977. Partial melting and electrical conductivities in the upper mantle. J. Geophys. Res. 82, 5409.

[70] Shankland, T.J., O'Connell, R.J., Waff, H.S., 1981. Geophysical constraints on partial melt in the upper mantle. Rev. Geophys. Space. Phys. 19, 394.

[71] Shankland, T.J., Duba, A., 1990. Standard electrical conductivity of isotropic, homogeneous olivine in the temperature range 1200-1500°C. Geophys. J. Int. 103, 25.

[72] Schock, R.N, Duba, A.G., Shankland, T.J., 1989. Electrical conduction in olivine. J. Geophys. Res. 94, 5829.

959 [73] Stacey, F.D., Anderson, D.L., 2001. Electrical and thermal conductivi-
960 ties of Fe-Ni-Si alloy under core conditions. Phys. Earth Planet. Inter. 124,
961 153.

962 [74] Stixrude, L., Lithgow-Bertelloni, C., 2005. Mineralogy and elasticity of
963 the oceanic upper mantle: Origin of the low-velocity zone. J. Geophys.
964 Res. 110, B03204, doi:10.1029/2004JB002965.

965 [75] ten Grotenhuis, S.M., Drury, M.R., Peach, C.J., Spiers, C.J., 2004. Elec-
966 trical properties of fine-grained olivine: Evidence for grain boundary trans-
967 port. J. Geophys. Res. 109, B06203, doi:10.1029/2003JB002799.

968 [76] Tarantola, A., Valette, B., 1982. Inverse problems=Quest for informa-
969 tion. J. Geophys. 50, 159.

970 [77] Tarits, P., Hautot, S., Perrier, F., 2004. Water in the mantle: Results
971 from electrical conductivity beneath French Alps. Geophys. Res. Lett. 31,
972 doi:10.1029/2003GL019277.

973 [78] Tarits, P., Mandea, M., 2010. The heterogeneous electrical conduc-
974 tivity structure of the lower mantle. Phys. Earth Planet. Int. 183,
975 doi:10.1016/j.pepi.2010.08.002.

976 [79] Tauzin, B., Debayle, E., Wittlinger, G., 2010. Seismic evidence for a
977 global low velocity layer in the Earth's upper mantle. Nature Geoscience
978 3, 718, doi:10.1038/NGEO969.

979 [80] Toffelmier, D.A., Tyburczy, J.A., 2007. Electromagnetic detection of a
980 410-km-deep melt layer in the Southwestern United States. Nature 447,
981 doi:10.1038/nature05922.

[81] Tyburczy, J.A., Fisler, D.K., 1995. Electrical properties of minerals and melts. In Ahrens, T.J. (Ed.). Mineral Physics and Crystallography: A Handbook of Physical Constants, AGU, Washington DC., 185.

[82] Tyburczy, J.A., Waff, H.S., 1983. Electrical conductivity of molten basalt and andesite to 25 kilobars pressure: Geophysical significance and implications for charge transport and melt structure. J. Geophys. Res. 88, 2413, doi:10.1029/JB088iB03p02413.

[83] Utada, H., Koyama, T., Shimizu, H., Chave, A.D., 2003. A semi-global reference model for electrical conductivity in the mid-mantle beneath the North Pacific region. Geophys. Res. Lett. 30, 1194, doi:10.1029/2002GL016092.

[84] Utada, H., Koyama, T., Obayashi, M., Fukao, Y., 2009. A joint interpretation of electromagnetic and seismic tomography models suggests the mantle transition zone below Europe is dry. Earth Planet. Sci. Lett., doi:10.1016/j.epsl.2009.02.027.

[85] Verhoeven, O., et al., 2009. Constraints on thermal state and composition of the Earth's lower mantle from electromagnetic impedances and seismic data. J. Geophys. Res. 114, B03302, doi:10.1029/2008JB005678.

[86] Waff, H.S., 1974. Theoretical considerations of electrical conductivity in a partially molten mantle and implications for geothermobarometry. J. Geophys. Res. 79, 4003.

[87] Wang., D., Mookherjee., M., Xu., Y., Karato, S.-I., 2006. The effect of water on the electrical conductivity in olivine. Nature 443, 977.

[88] Watson, H.C., Roberts, J.J., Tyburczy, J.A., 2010. Effect of conductive impurities on electrical conductivity in polycrystalline olivine. Geophys. Res. Lett. 37, L02302, doi:10.1029/2009GL041566.

[89] Watt J.P., Davies, G.F., O'Connell, R.J., 1976. The elastic properties of composite materials. Rev. Geophys. Space Phys. 14, 541.

[90] Weidelt, P., 1972. The inverse problem of geomagnetic induction, Z. Geophys. 38, 257, 1972.

[91] Wood, B. J., 1995. The effect of H_2O on the 410-kilometer seismic discontinuity. Science 268, 71.

[92] Wu, X., et al., 2010. Electrical conductivity measurements of periclase under high pressure and high temperature. Physica B 405, doi:10.1016/j.physb.2009.08.036.

[93] Xu, Y., McCammon, C., Poe, B.T., 1998. The effect of alumina on the electrical conductivity of silicate perovskite. Science 282, 922.

[94] Xu, Y., Shankland, T.J. 1999. Electrical conductivity of orthopyroxene and its high pressure phases. Geophys. Res. Lett. 26, 2645.

[95] Xu, Y., Shankland, T.J., Poe, B.T., 2000. Laboratory-based electrical conductivity in the Earth's mantle. J. Geophys. Res. 108, 2314.

[96] Xu, W., Lithgow-Bertelloni, C., Stixrude, L., Ritsema, J., 2008. The effect of bulk composition and temperature on mantle seismic structure. Earth Planet. Sci. Lett., doi:10.1016/j.epsl.2008.08.012.

[97] Yoshino, T., 2010. Laboratory electrical conductivity measurements of mantle minerals. Surv. Geophys., 31., 163.

[98] Yoshino, T., Matsuzaki, T., Yamashita, S., Katsura, T., 2006. Hydrous olivine unable to account for conductivity anomaly at the top of the asthenosphere. Nature 443, doi:10.1038/nautre05223.

[99] Yoshino, T., Nishi, M., Matsuzaki, T., Yamazaki, D., Katsura, T., 2008a. Electrical conductivity of majorite garnet and its implications for electrical structure in the mantle transition zone. Phys. Earth Planet. Int., doi:10.1016/j.pepi.2008.04.009.

[100] Yoshino, T., Manthilake, G., Matsuzaki, T., Katsura, T., 2008b. Dry mantle transition zone inferred from the conductivity of wadsleyite and ringwoodite. Nature 451, doi:10.1038/nautre06427.

[101] Yoshino, T., Katsura, T., 2009a. Reply to Comments on "Electrical conductivity of wadsleyite as a function of temperature and water content" by Manthilake et al. Phys. Earth Planet. Int., doi:10.1016/j.pepi.2009.01.012.

[102] Yoshino, T., Katsura, T., 2009b. Effect of iron content on electrical conductivity of ringwoodite, with implications for electrical structure in the transition zone. Phys. Earth Planet. Int., doi:10.1016/j.pepi.2008.09.015.

[103] Yoshino, T., Matsuzaki, T., Shatskiy, A., Katsura, T., 2009. The effect of water on the electrical conductivity of olivine aggregates and its implications for the electrical structure of the upper mantle. Earth Planet. Sci. Lett., doi:10.1016/j.epsl.2009.09.032.

[104] Yoshino, T., Laumonier, M., McIsaac, E., Katsura, T., 2010. Electrical conductivity of basaltic and carbonatite melt-bearing peridotites at high pressures: Implications for melt distribution and melt fraction in the upper mantle. Earth Planet. Science Lett., doi:10.1016/j.epsl.2010.04.050.

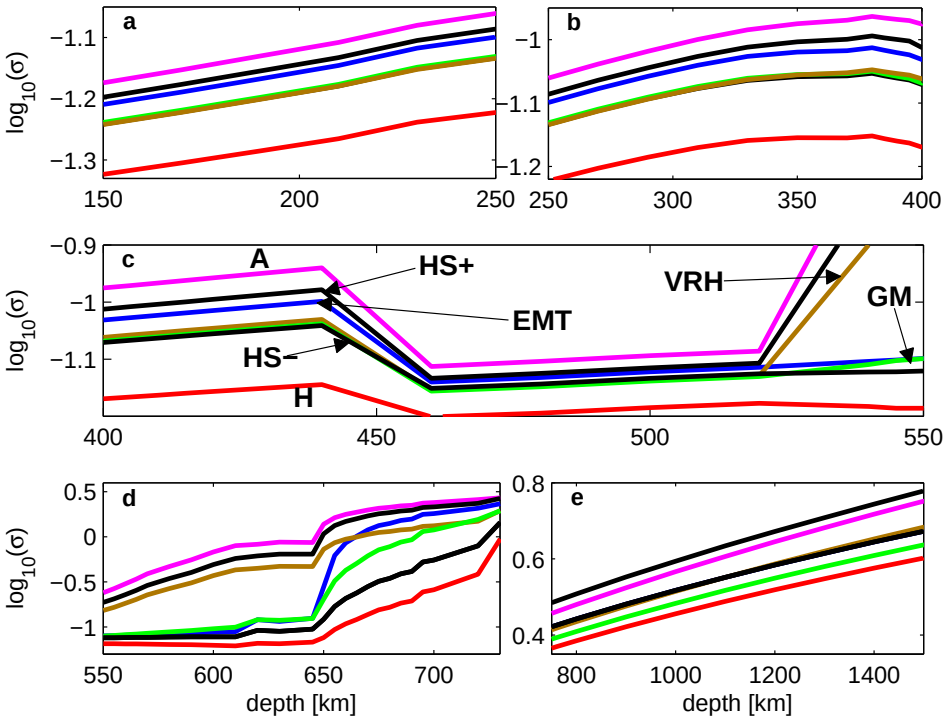

Figure 1: Estimated bulk conductivity profiles using different averaging schemes (see main text for details) in the upper mantle (a,b), transition zone (c,d) and lower mantle (e). Colour coding is the same in all plots. The following averages are shown: A - arithmetic mean; H - harmonic mean; HS- - lower Hashin-Shtrikman bound; HS+ - upper Hashin-Shtrikman bound; EMT - effective medium theory; VRH - Voigt-Reuss-Hill average; and GM - geometric mean. In (a) and (b) HS- is hidden behind the GM and VRH profiles.

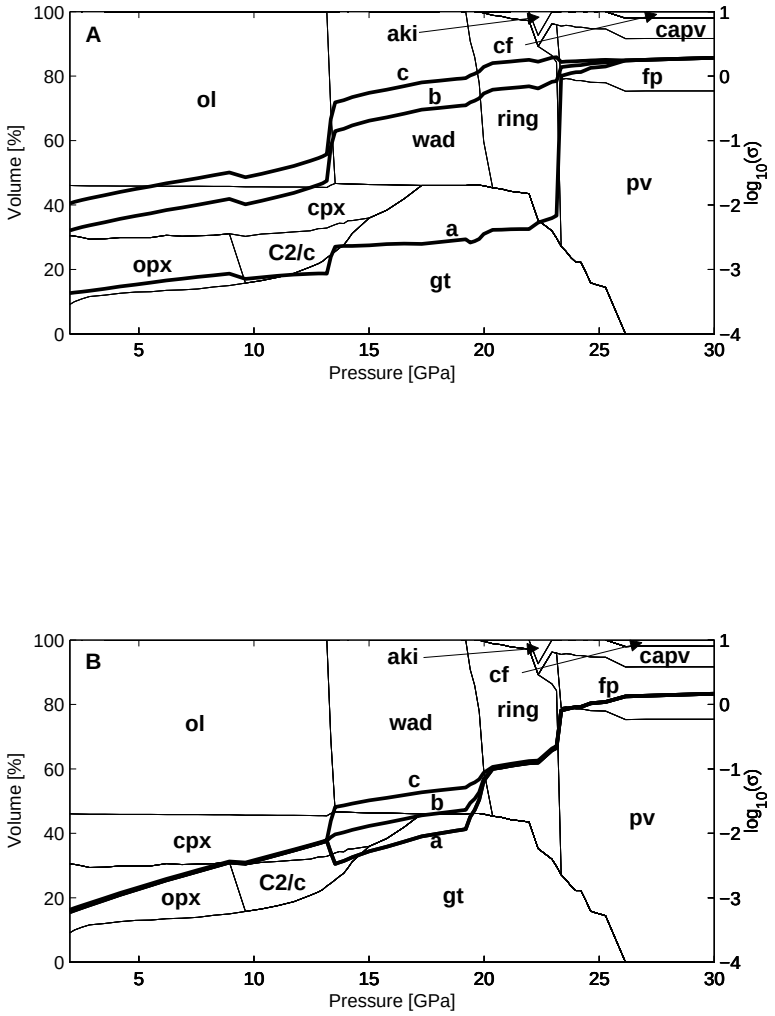

Figure 2: Bulk conductivity profiles as a function of water content in the upper mantle, transition zone, and uppermost lower mantle. Conductivity profiles in plots (A) and (B) were constructed using the KD and YK conductivity databases, respectively. In both plots water content in the upper mantle (UM) and transition zone (TZ) is: (a) both 0 wt% water, i.e., "dry" conditions, (b) 0.001 wt% (UM), and 0.1 wt% (TZ) and (c) 0.005 wt% (UM) and 0.5 wt% (TZ). Note that the KD database does not contain a conductivity term for ringwoodite at "dry" conditions; for these calculations we included a vanishingly small amount of water (0.0001 wt%). Phases are (mineral abbreviations defined in the main text): ol, opx, cpx, C2/c, gt, wad, ring, aki, ca-pv, fp, pv, and cf.

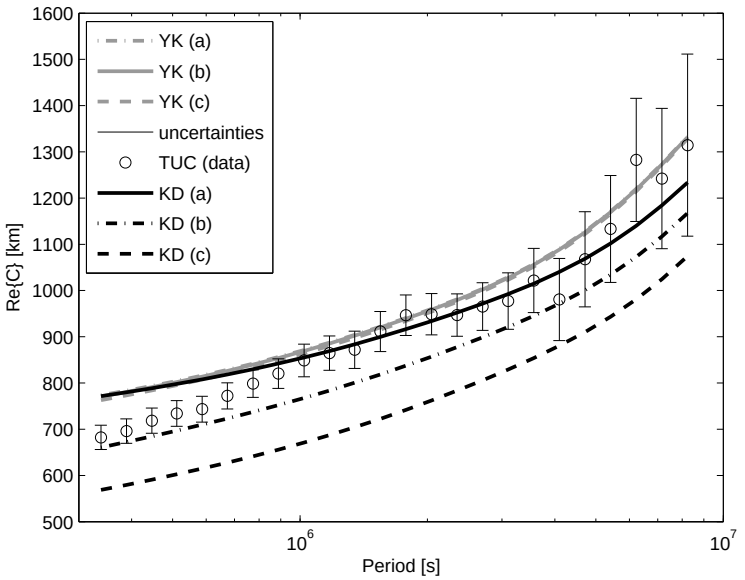

Figure 3: Inductive response functions (real part only) calculated for the six conductivity profiles shown in figure 2 and compared to observations from station TUC. KD and YK refer to the laboratory databases used for modelling conductivity profiles. (a), (b), and (c) refer to the same compositions as in the previous figure.

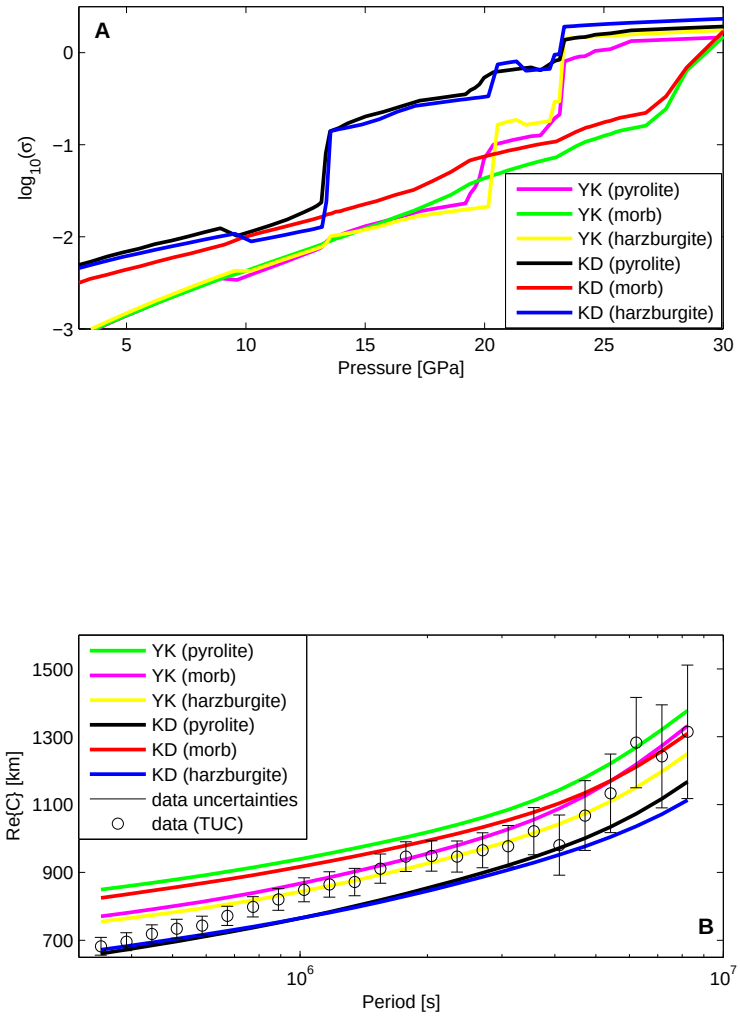

Figure 4: Dependence of conductivity and response functions on mantle composition. (A) Bulk conductivity profiles for three different compositions in the upper mantle, transition zone, and outermost lower mantle (table 9) using the two conductivity databases KD and YK. (B) Inductive response functions (real part only) for the six profiles shown in (A) and compared to observations from station TUC. "Dry" mantle conditions are assumed.

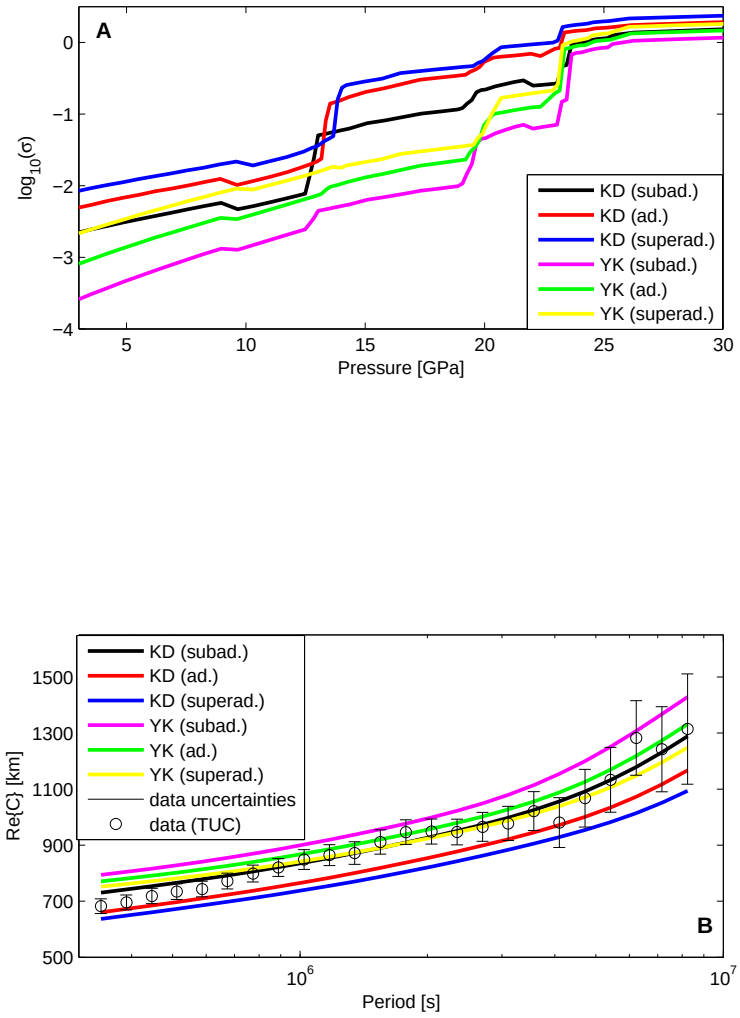

Figure 5: Dependence of conductivity and response functions on mantle geotherm. (A) Bulk conductivity profiles for three different geotherms, comprising "subadiabatic", adiabatic, and "superadiabatic" mantle conditions from the lithosphere down to the outermost lower mantle using the conductivity databases KD and YK. (B) Inductive response functions (real part only) for the six profiles shown in (A) and compared to observations from station TUC. "Dry" mantle conditions are assumed.

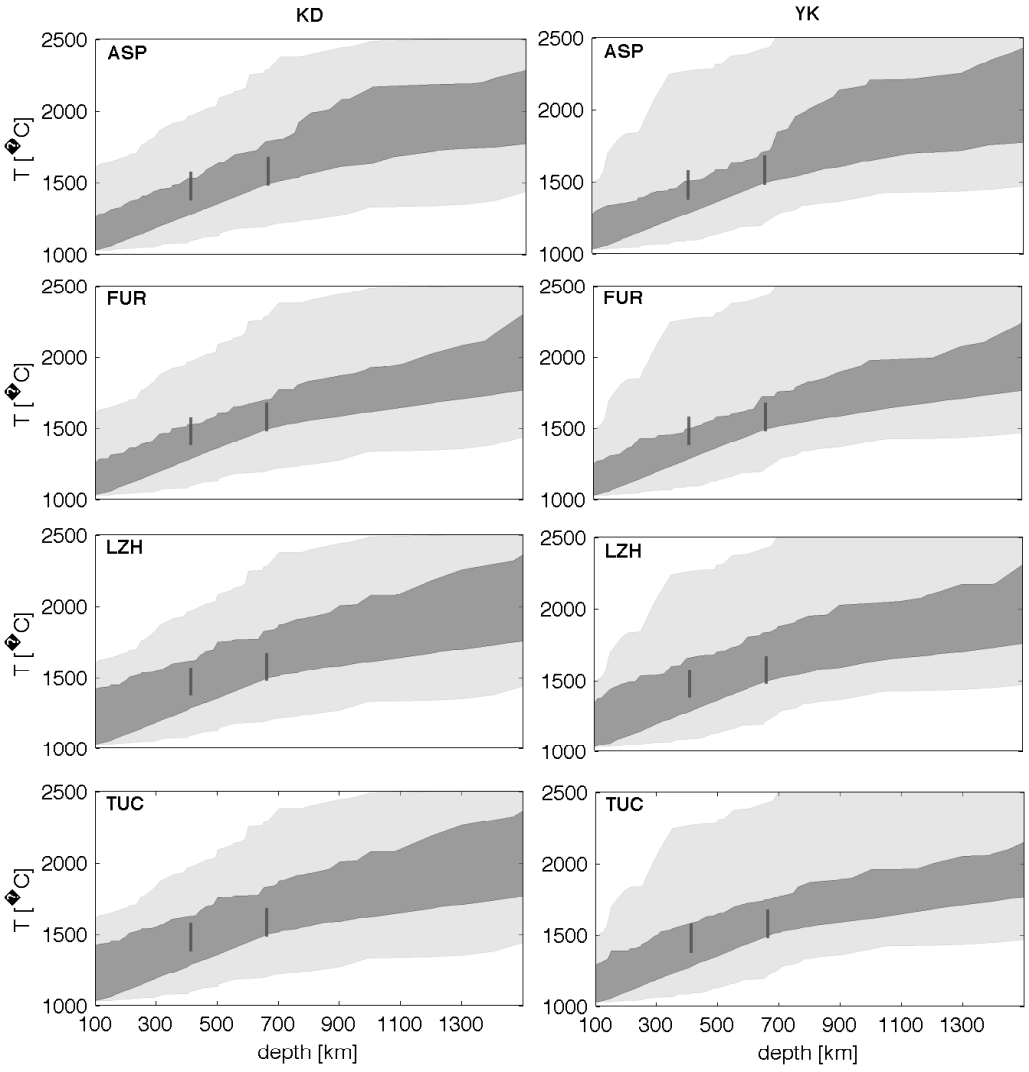

Figure 6: Sampled prior and posterior geotherms beneath stations ASP, FUR, LZH, and TUC (observatories are defined in the main text) obtained using the KD (left column) and YK (right column) databases, respectively. Profiles include the entire range of sampled thermal models. Range of prior geotherms are given by light gray shading. Solid vertical bars indicate experimentally determined temperatures for the major mineral phase reactions at 410 and 660 km depth. See text for details.

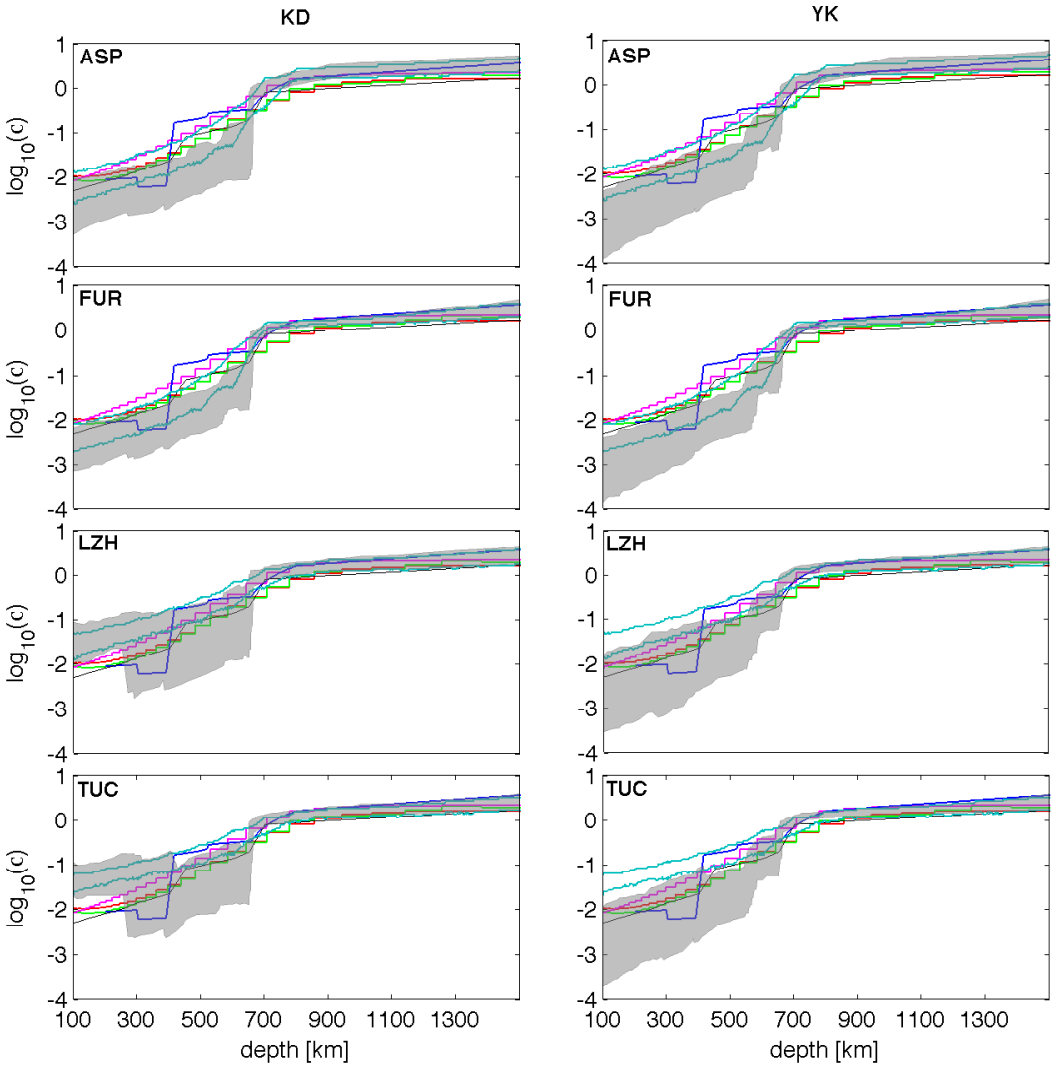

Figure 7: Sampled posterior electrical conductivity profiles beneath stations ASP, FUR, LZH, and TUC (observatories are defined in the main text) obtained using the KD (left column) and YK (right column) conductivity databases, respectively. Profiles include the entire range of sampled conductivity models. For comparison some previous one-dimensional conductivity profiles are shown (thin lines): red - Olsen (1999); blue - Kuvshinov and Olsen (2006); black - Xu et al. (2000); magenta - Khan et al. (2006); light blue - upper and lower limit of the range of models (95% credible interval) from Khan et al. (2011).

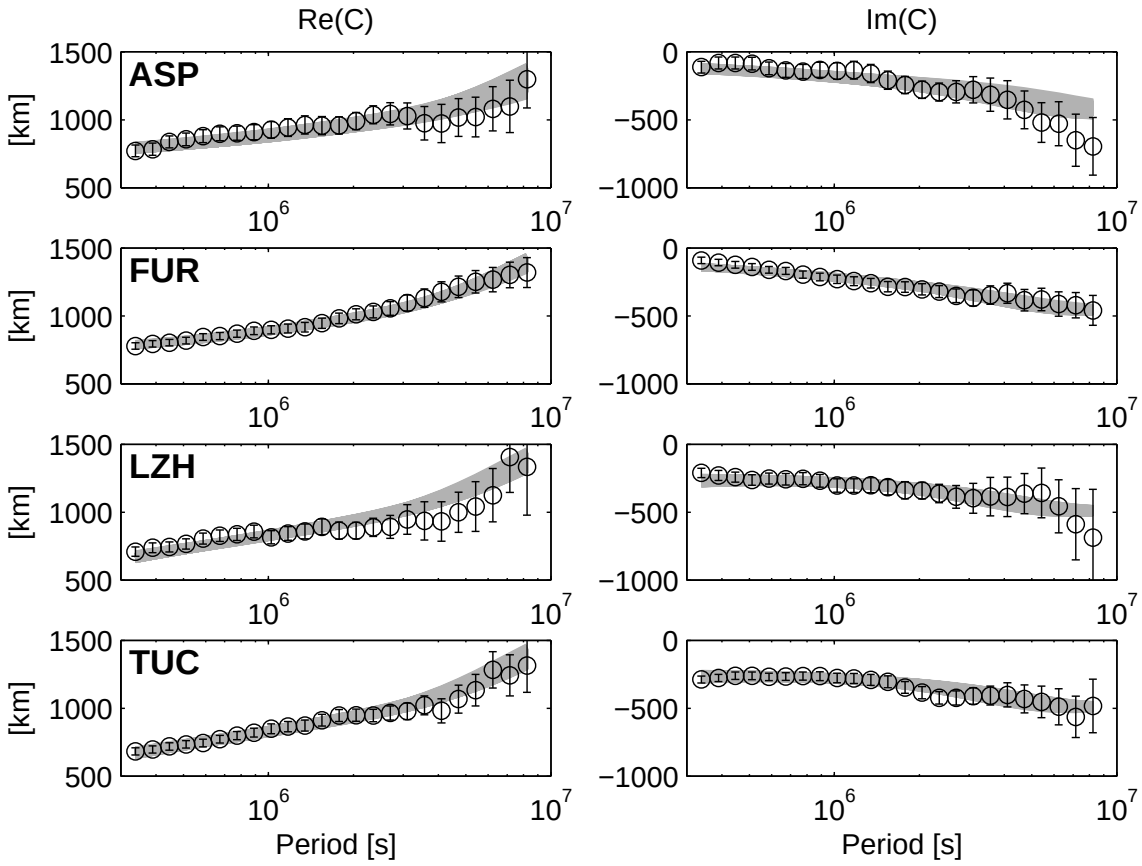

Figure 8: Fit to inductive response functions (observed data - circles) and uncertainties (bars) from four geomagnetic observatories using the KD-based conductivity profiles in figure 7A–B (shaded bands - calculated data). Left and right columns depict real and imaginary parts of C-responses, respectively.

Observatories are defined in the main text.

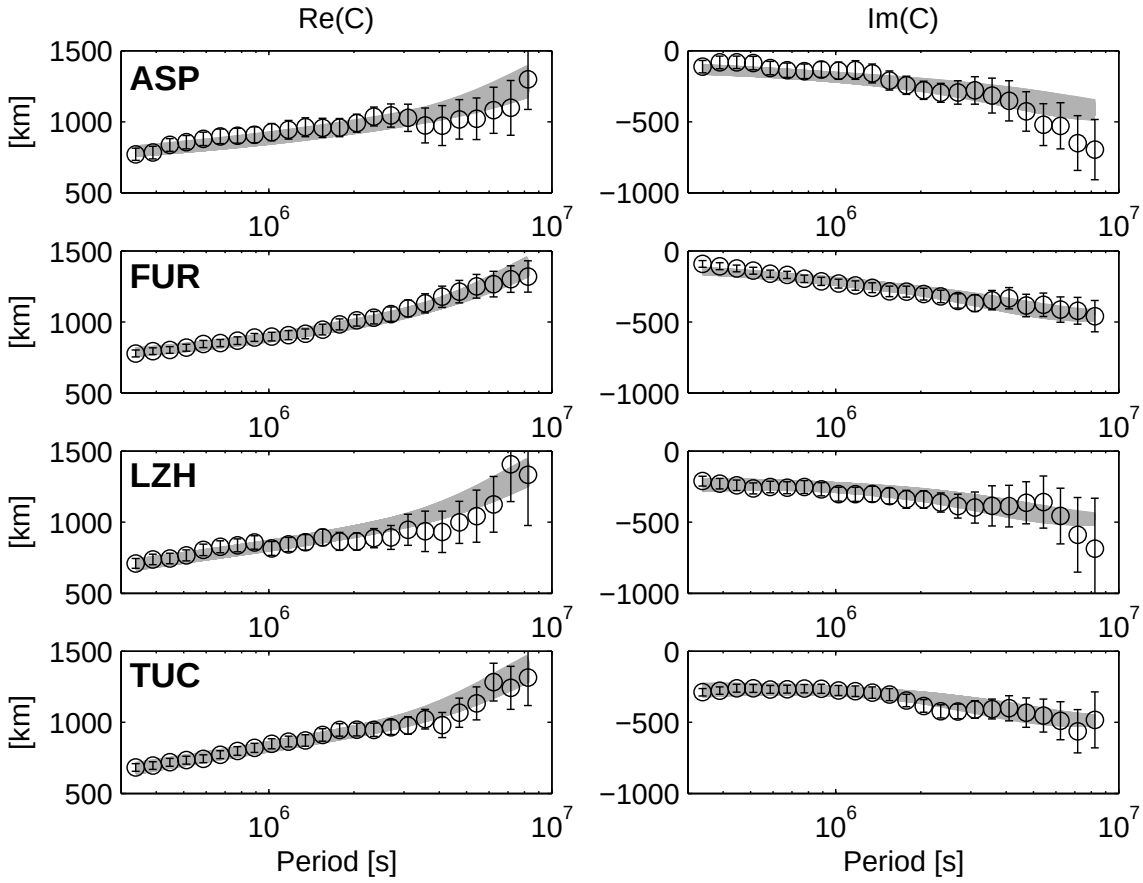

Figure 9: Fit to inductive response functions (observed data - circles) and uncertainties (bars) from four geomagnetic observatories using the YK-based conductivity profiles in figure 7C–D (shaded bands - calculated data). Left and right columns depict real and imaginary parts of C-responses, respectively.

Observatories are defined in the main text.

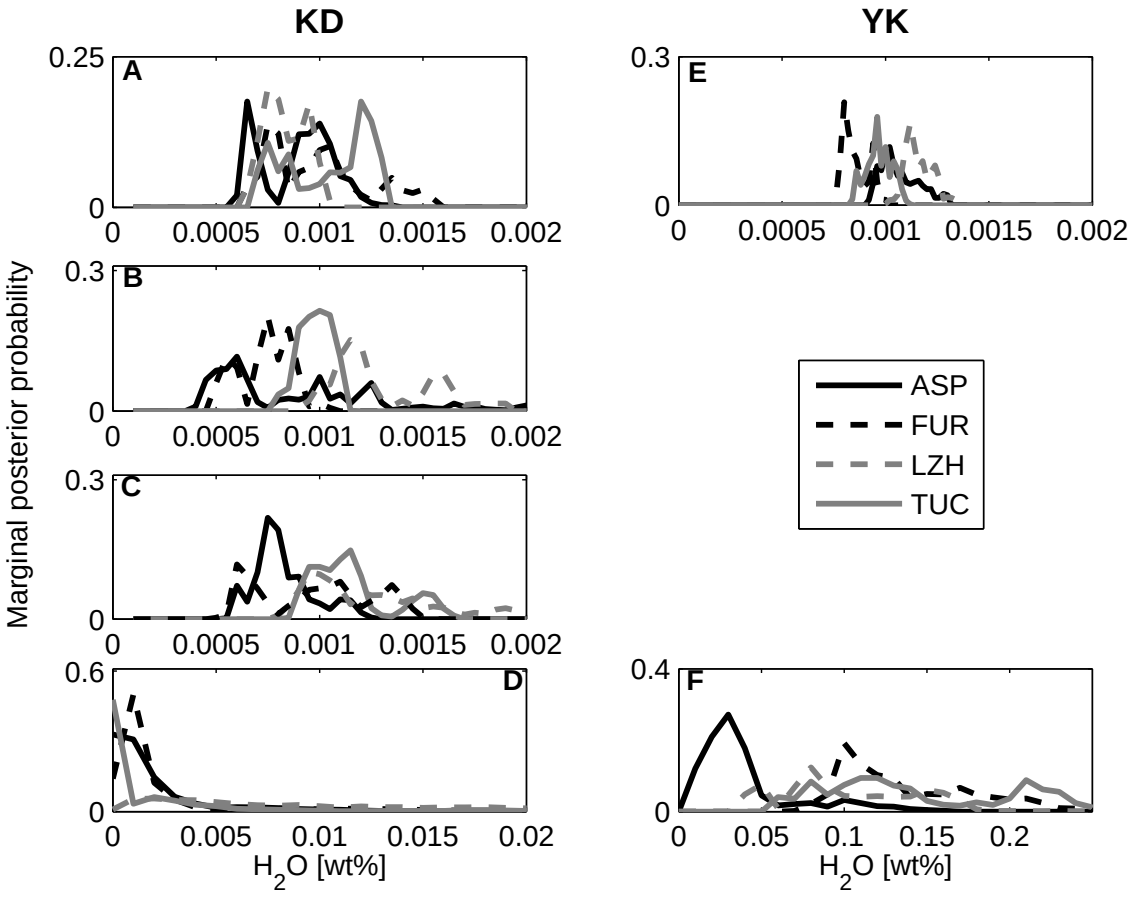

Figure 10: Sampled water contents in the upper mantle and transition zone. as marginal posterior probability distributions. Letters above plots refer to the two conductivity databases used - KD (Karato, Dai and coworkers) and YK (Yoshino, Katsura and coworkers). (A,E) olivine, (B) orthopyroxene, (C) garnet, and (D,F) wadsleyite and ringwoodite, Only part of the sampled range of water contents is displayed; the full prior range encompassed 0 to 1 wt%).